Gravitational recoil from binary black hole mergers: The close-limit approximation

Carlos F. Sopuerta,[1,2] Nicolás Yunes,[1,3] and Pablo Laguna[1,2,3]

[1]*Institute for Gravitational Physics and Geometry and Center for Gravitational Wave Physics, The Pennsylvania State University, University Park, Pennsylvania 16802, USA*
[2]*Department of Astronomy & Astrophysics, The Pennsylvania State University, University Park, Pennsylvania 16802, USA*
[3]*Department of Physics, The Pennsylvania State University, University Park, Pennsylvania 16802, USA*

The coalescence of a binary black hole system is one of the main sources of gravitational waves that present and future detectors will study. Apart from the energy and angular momentum that these waves carry, for unequal-mass binaries there is also a net flux of linear momentum that implies a recoil velocity of the resulting final black hole in the opposite direction. Due to the relevance of this phenomenon in astrophysics, in particular, for galaxy merger scenarios, there have been several attempts to estimate the magnitude of this velocity. Since the main contribution to the recoil comes from the last orbit and plunge, an approximation valid at the last stage of coalescence is well motivated for this type of calculation. In this paper, we present a computation of the recoil velocity based on the close-limit approximation scheme, which gives excellent results for head-on and grazing collisions of black holes when compared to full numerical relativistic calculations. We obtain a maximum recoil velocity of ~ 57 km/s for a symmetric mass ratio $\eta = M_1 M_2/(M_1 + M_2)^2 \sim 0.19$ and an initial proper separation of $4M$, where M is the total Arnowitt-Deser-Misner (ADM) mass of the system. This separation is the maximum at which the close-limit approximation is expected to provide accurate results. Therefore, it cannot account for the contributions due to inspiral and initial merger. If we supplement this estimate with post-Newtonian (PN) calculations up to the innermost stable circular orbit, we obtain a lower bound for the recoil velocity, with a maximum around 80 km/s. This is a lower bound because it neglects the initial merger phase. We can however obtain a rough estimate by using PN methods or the close-limit approximation. Since both methods are known to overestimate the amount of radiation, we obtain in this way an upper bound for the recoil with maxima in the range of 214–240 km/s. We also provide nonlinear fits to these estimated upper and lower bounds. These estimates are subject to uncertainties related to issues such as the choice of initial data and higher effects in perturbation theory. Nonetheless, our estimates are consistent with previous results in the literature and suggest a narrower range of possible recoil velocities.

I. INTRODUCTION

The inspiral and merger of binary black holes systems is one of the most interesting sources of gravitational waves that both earth-based interferometric antennas (LIGO [1], VIRGO [2], GEO600 [3], and TAMA [4]) and space-based ones (LISA [5]) will detect. These waves carry both energy and momentum away from the system, leading to the adiabatic shrinking of the orbit, due to the former, and a recoil of the merged object by conservation of momentum, due to the latter. The magnitude of this recoil is of astrophysical importance because it determines whether the merged hole will be ejected from its host galaxy.

Possible observational evidence for such a recoil may be the observations of faint galaxies [6,7] where the lack of a dense nucleus has been associated with the central black hole being ejected after merger [8]. There is also evidence of an ejection of a supermassive black hole in ongoing galaxy mergers, either because of recoil or because of slingshot due to the presence of 3 or more supermassive black holes in the merger [9]. The gravitational recoil has also been shown to have important consequences in hierarchical merging scenarios and the observable structure of galaxy nuclei. Recoil velocities of a few hundred km/s

could be large when compared to escape velocities of dwarf galaxies, globular clusters, and dark matter halos [8,10]. For supermassive black holes at the centers of galaxies, a kick of this magnitude could potentially transfer energy to the stars in the nucleus [8]. There are thus very important astrophysical aspects that can be refined or clarified with a better understanding of the black hole kicking process.

Mass distributions without symmetries that undergo gravitational collapse of any sort will exhibit momentum ejection and recoil of the center of mass of the remnant due to the strong emission of gravitational radiation [11–15]. Of particular interest is the case of unequal-mass black hole binary systems. An intuitive picture of how the system gets a *kick* after the merger is the following [16,17]: From the *center of mass* point of view, the lighter black hole will move faster than the heavier one, and hence it will beam forward gravitational radiation stronger. Then, there will be a net flux of linear momentum carried by the gravitational radiation in the direction of the lighter black hole, and this will cause a recoil of the center of mass in the opposite direction. The first analytic studies of this subject were carried out by Fitchett and Detweiler [18,19]; Oohara and Nakamura [20]; Nakamura and Haugan [21]; and

Wiseman [16]. Because of the strong nonlinearity of the merger phase, analytic studies have difficulties in obtaining an accurate estimate of the recoil velocity. The first quasi-Newtonian analytic calculations were presented in [18,19], while a post-Newtonian (PN) analysis has been carried out in [16,22,23]. Estimates using black hole perturbation theory have been given in [17,24], and an estimate that combines full numerical relativity and perturbation theory, the *Lazarus* approach, is given in [25].

Full numerical relativistic simulations are a natural approach to this problem since they can in principle handle the nonlinearities of the gravitational field during the merger. The challenge is the resolution that the computational resources impose. Some calculations have already been carried out in different scenarios to estimate recoil velocities. The first one was done by Anninos and Brandt [26] for the case of the head-on collision of two unequal-mass black holes. Their numerical calculations were effectively 2-dimensional since they made use of the axisymmetry of the configuration. Using the same type of numerical calculations they also estimated the gravitational radiation recoil from highly distorted black holes [27]. More recently, and due to the significant advances in 3-dimensional numerical relativity in the binary black hole problem [28–30], estimates of the radiation recoil velocity have also appeared [31,32].

Each of the approaches described above has its own limitations. Analytic approaches are able to provide accurate estimates in their region of validity. However, the largest contribution to the recoil velocity occurs during merger, precisely where the approximation methods break down. Numerical simulations, in principle, have the opportunity of producing estimates with a minimal number of assumptions. However, as we have mentioned, these calculations have also limitations and use initial data that is only an approximation to the actual astrophysical configurations. Therefore, the error bars on the computed distribution of recoil velocities relative to the distribution present in nature are believed to be large and, even worse, are difficult to estimate. It is then not surprising to find disagreements on the estimated recoil velocity as calculated with different methods.

In this paper, we present estimates of the recoil velocity using an approach not used before, the close-limit approximation (CLA), which combines both analytical and numerical techniques. The CLA was introduced by Price and Pullin [33], who showed that this approximation method provides accurate results compared to those obtained from numerical relativity [34] for head-on collisions of two black holes (see also [35]). The CLA scheme is based on the assumption that in the last stage of coalescence, when the black holes are sufficiently *close* to each other, the system behaves, up to a certain degree of approximation, as a single distorted hole. Then, the CLA scheme consists of establishing an appropriate correspondence between the

binary black hole system and a single perturbed hole. Once this correspondence is made, one can extract initial data that can be evolved by the perturbative relativistic equations. From the outcome of the evolution, one can estimate the fluxes of energy, angular momentum, and linear momentum carried away to spatial infinity by the gravitational radiation emitted. The CLA scheme has been developed and applied by a number of authors [36–43]. In particular, Andrade and Price [44] used the CLA to estimate the recoil velocity of a head-on collision of unequal-mass black holes starting from rest.

Since the CLA applies to the last stage of the merger of two black holes, it is very appealing to use it to estimate the recoil velocity of the merger of an unequal-mass black hole binary system. With this scheme, we obtain a maximum recoil velocity of $\sim\{17, 31, 57\}$ km/s for a symmetric mass ratio $\eta = M_1 M_2/(M_1 + M_2)^2 \sim 0.19$ and initial proper separations of $\{3, 3.5, 4\}M$, with M the total Arnowitt-Deser-Misner (ADM) mass. Beyond a proper separation of $4M$ the CLA is not expected to provide accurate results [44]. Therefore, this method cannot account for the contributions during the inspiral and initial merger phase. Supplementing this estimate with PN calculations up to the innermost stable circular orbit (ISCO), we obtain a lower bound for the recoil velocity, with a maximum of $\sim$80 km/s. This lower bound neglects the initial merger phase, for which we can obtain an approximate estimate by using either PN methods or the CLA. Since both methods are known to overestimate the amount of radiation during the early merger phase, we obtain, thus, an upper limit for the recoil with maxima in the range of 214–240 km/s. We also perform nonlinear fits to these bounds and obtain

$$v_{\text{fit}} = a\eta^2\sqrt{1 - 4\eta}(1 + b\eta + c\eta^2), \tag{1}$$

where $a = 6907$ km/s, $b = -2.46$, and $c = 3.03$ for the lower bound and $a = 13\,927$ km/s, $b = -1.10$, and $c = 1.55$ for the upper bound.

The plan of this paper is as follows: Sec. II describes the main procedure of our calculation; Sec. III constructs initial data for a quasicircular binary black hole system in the 3 + 1-formalism; Sec. IV maps these initial data to a single perturbed black hole spacetime, such that it is suitable for a CLA evolution; Sec. V describes the numerical implementation and presents results from the evolution within the CLA scheme; Sec. VI estimates the lower and upper bounds, as well as constructing the nonlinear fits to these bounds; we finish in Sec. VII with a summary and discussion of the main results and points to future research to obtain improved estimates.

The conventions that we use throughout this work are the following: For the 4-dimensional spacetime, we use Greek letters for the indices and a semicolon for the covariant derivative. The Schwarzschild metric admits a 2 + 2 decomposition consisting of the warped product of a Lorentzian 2-dimensional manifold with the 2-sphere (see

[45,46]). On the 2-dimensional Lorentzian manifold indices are denoted by capital Latin letters, the covariant derivative associated with the 2-dimensional metric is represented by a vertical bar, and the Levi-Civita antisymmetric tensor by ϵ_{AB}. On the 2-sphere indices are denoted by the lowercase Latin letters $a, b, \ldots, h$, the covariant derivate by a colon, and the Levi-Civita antisymmetric tensor by ϵ_{ab}. When using the $3 + 1$ decomposition of spacetime quantities, spatial indices are denoted by the lowercase Latin letters $i, j, k, \ldots$. Uncontrolled remainders are denoted with $\mathcal{O}(A)$ or $\mathcal{O}(A, B)$, which stands for terms of order A and terms of order A or B, respectively. Although usually, when dealing with order symbols, A and B must be dimensionless, here they will not be, but can be made to be dimensionless through division by the appropriate factor. We also use physical units in which $G = c = 1$.

II. DESCRIPTION OF OUR CALCULATION

In this paper, we use the CLA scheme to calculate the recoil velocities after the merger of an unequal-mass binary black hole system. Because of the complexity of the calculation, we discuss here the different steps involved, while getting a glimpse of the general scheme. First, we need to construct initial data corresponding to a nonspinning binary black hole system in quasicircular orbital motion. The method employed to construct the data is the standard one: we solve the constraints on an initial slice using the York-Lichnerowicz conformal decomposition. Then, the solution needs to be expanded in two parameters: the separation of the two black holes, based on the main assumption of the CLA, that is, small separation between the holes; and their linear momenta, rooted in an additional *slow-motion* approximation [47].

The second step is to establish a map between this initial data and the generic initial data corresponding to a perturbed single black hole. In this work we only consider the case in which the single black hole is a nonrotating Schwarzschild hole. There is also the possibility of considering a Kerr black hole (see [47] for details), but the CLA machinery in that case is more intricate. After expanding the initial data in the separation and linear momenta, it is straightforward, after some coordinate changes, to identify a Schwarzschild background and its perturbations.

Once the perturbations have been identified, we need to calculate initial data suitable for evolving the linearized (around the Schwarzschild background) Einstein equations. The spherical symmetry of the background allows us to separate the linearized equations. Then, by decomposing the perturbations in spherical harmonics we obtain decoupled equations for each mode. Moreover, by appropriately reparametrizing the perturbations, we can decouple the equations for each individual mode, so that the problem reduces to solving a master equation for a

complex combination of the metric perturbations. These master equations (usually known as the Regge-Wheeler and Zerilli-Moncrief equations) are 1-dimensional wavetype equations containing a potential that accounts for the effect of the background spacetime curvature. Therefore, the problem of providing initial data reduces to finding initial conditions for these master functions.

The initial data contains three parameters that we need to specify. These parameters are associated with the initial distance between the holes, the mass ratio, and the initial linear momentum. The mass ratio is an independent parameter that will be used to study the functional behavior of the recoil velocity. The distance and linear momentum parameters determine the dynamical character of the binary and, therefore, they must be chosen carefully. To that end, we use the standard method of minimizing the binding energy of the system, so that the binary is in a quasicircular orbit. The expressions that we obtain are formally the same as in Newtonian theory, although they cannot be assigned the same interpretation, since they are expressed in terms of *bare* parameters. In order to relate these parameters to meaningful physical ones, we must introduce a proper separation and a physical mass ratio. The proper separation can be calculated by evaluating the minimum proper distance between the marginally trapped surfaces surrounding each individual hole.

The final step is to solve the master equations and evaluate the different physical quantities of interest. The metric waveforms h_+ and $h_\times$, together with the fluxes of energy, angular and linear momentum carried away by gravitational waves can be computed in terms of the master functions and their first time derivatives. In this paper, we include the general formulae for the linear momentum fluxes in terms of the perturbation master functions. We present several plots of these quantities, together with plots of the recoil velocities for different initial separations.

III. INITIAL DATA

In this section, we begin the initial data construction for an unequal-mass binary black hole system suitable to the CLA scheme. To that end, we extend the results of Andrade and Price [44], who carried out the calculation for unboosted head-on collisions, and also extend the results of Khanna *et al.* [47], who constructed data for equal-mass black holes in a quasicircular orbit. Our calculation not only allows for arbitrary mass ratios, but it also includes higher-order terms in the expansion of the initial data, which are essential in the calculation of the recoil.

In order to solve the Hamiltonian and momentum constraints, we use the conformal transverse-traceless method of Lichnerowicz, York, and others [48–52]. The 3-metric γ_{ij} is decomposed in terms of a conformal factor Φ and an auxiliary metric $\hat{\gamma}_{ij}$, $\gamma_{ij} = \Phi^4 \hat{\gamma}_{ij}$, which here we assume to be conformally flat:

$$ds^2 = \gamma_{ij}dx^i dx^j = \Phi^4(dR^2 + R^2 d\Omega^2), \qquad (2)$$

where $d\Omega^2 = d\theta^2 + \sin^2\theta d\varphi^2$ is the line element of the 2-sphere. For the extrinsic curvature K_{ij}, we choose a *maximal* initial slice, that is, K_{ij} is trace free: $\gamma^{ij}K_{ij} = 0$. Then, we also conformally decompose the trace-free extrinsic curvature K_{ij} as

$$K_{ij} = \Phi^{-2}\hat{K}_{ij}, \qquad (3)$$

and we further make the choice that the longitudinal part of $\hat{K}_{ij}$ vanishes, so that $\hat{K}_{ij}$ is a symmetric transverse-traceless tensor. Then, the momentum and Hamiltonian constraints reduce to

$$\hat{\nabla}^j \hat{K}_{ji} = 0, \qquad (4)$$

$$\hat{\nabla}^2\Phi = -\tfrac{1}{8}\Phi^{-7}\hat{K}_{ij}\hat{K}^{ij}, \qquad (5)$$

where $\hat{\nabla}_i$ and $\hat{\nabla}^2$ denote the covariant derivative and Laplacian associated with the flat 3-metric $\hat{\gamma}_{ij}$. The momentum constraint [Eq. (4)] can be exactly solved using the method of Bowen and York [53]. For a single black hole located at $R = R_o$ with linear momentum P it can be written as follows:

$$\hat{K}_{ij}^{\text{one}} = \frac{3}{2|R - R_o|^2}[2P_{(i}n_{j)} - (\hat{\gamma}_{ij} - n_i n_j)P^k n_k], \quad (6)$$

P^i is the ADM momentum of a single hole, while n^i is a unit vector in flat 3-dimensional space directed from the location of the single hole to an arbitrary point, namely

$$n^i = \frac{R^i - R_o^i}{|R - R_o|}, \qquad (7)$$

and the vertical bars, $|\cdot|$, denote the norm of vector in the flat 3-dimensional space. In order to construct a solution for two holes, we can simply superpose two solutions of the type of Eq. (6).

Before constructing the extrinsic curvature, it will be useful to first describe the initial physical configuration. The system we are modeling consists of two black holes with masses M_1 and M_2 located on the X-axis, a coordinate distance d apart, as shown in Fig. 1. In this figure. R_1, R_2, and R are radial vectors that point from the origin to hole 1, hole 2, and an arbitrary point, respectively. Moreover, $R_{12} = R_2 - R_1$ is also a vector that points from hole 1 to 2, and P and $-P$ are the linear momenta associated with holes 1 and 2, respectively. Since the linear momenta are parallel to the Y-axis, the orbital angular momentum is directed along the Z-axis. With such a physical scenario, the solution of Eq. (4) can be written as (see also [47]):

$$\hat{K}_{ij} = \hat{K}_{ij}^{\text{one}}[R_0 = R_1, P] + \hat{K}_{ij}^{\text{one}}[R_o = R_2, -P], \quad (8)$$

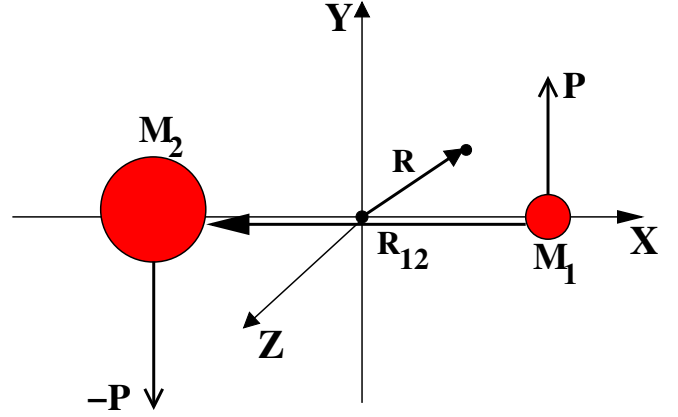where we have defined $P = P\hat{y}$. The ADM momentum

FIG. 1 (color online). Schematic diagram of the initial physical configuration. The linear momenta are parallel to the Y-axis and span the X-Y plane, so that the angular momentum is aligned with the Z-axis.

corresponding to $\hat{K}_{ij}^{\text{one}}$ is simply P and the one associated with $\hat{K}_{ij}$ is zero.

Let us now concentrate on the solution to the Hamiltonian constraint. Using Eq. (8) in the Hamiltonian constraint leads to a source term quadratic in P. We now introduce a slow-motion approximation, where we assume that the linear momentum P is *small*, in the sense that terms of $\mathcal{O}(v^2)$ are much smaller than terms of $\mathcal{O}(v)$, where v is a measure of the orbital velocity. We, thus, neglect terms of $\mathcal{O}(P^2)$, so that the Hamiltonian constraint reduces to the Laplace equation

$$\nabla^2\Phi = 0. \qquad (9)$$

The solution of this equation depends on our choice of topology. If we choose the initial slice to have a single asymptotically flat region, the solution to the conformal factor is the Misner solution [54], but if one chooses the slice to have three asymptotically flat regions, the solution is the Brill-Lindquist [55] one. In this paper, we adopt the latter and the conformal factor takes the form of the Newtonian potential:

$$\Phi = 1 + \frac{m_1}{2|R - R_1|} + \frac{m_2}{2|R - R_2|}, \qquad (10)$$

where m_1 and m_2 denote the bare masses of each individual hole. One reason for choosing the Brill-Lindquist (BL) solution is that it is simpler to manipulate, while it has also been shown [44] to lead to essentially the same results when calculating recoil velocities for head-on collisions. We remark that, although terms of $\mathcal{O}(P^2)$ have been neglected, they can be straightforwardly added in a perturbative fashion, but this will be studied elsewhere.

Let us comment further on the topology of the initial slice associated with the BL solution, as it is important in some calculations. As we have already mentioned, this solution has three asymptotically flat regions: one of

them, Σ_0, corresponds to the region far from the two holes, $R = |\boldsymbol{R}| \gg |\boldsymbol{R}_1| = R_1$ and $R \gg |\boldsymbol{R}_2| = R_2$; the other two, Σ_1 and Σ_2, are associated with hole 1 and 2, respectively. By simple inspection of the conformal factor [Eq. (10)], the solution seems ill-behaved at the location of the holes, $\boldsymbol{R} = \boldsymbol{R}_1$ and $\boldsymbol{R} = \boldsymbol{R}_2$, although it is actually not. Near each hole, the geometry is invariant under the transformation: $|\boldsymbol{R} - \boldsymbol{R}_\Lambda| \to m_\Lambda^2/(4R'_\Lambda)$ ($\Lambda = 1, 2$). The value $m_\Lambda/2$ coincides with the intersection of the event horizon with the initial slice for a single hole and it is a fixed point in the transformation. This value is sometimes referred to as the *throat*, joining two asymptotically flat regions. Therefore, the points $\boldsymbol{R} = \boldsymbol{R}_1$ and $\boldsymbol{R} = \boldsymbol{R}_2$ are just an *image* of the infinities of Σ_1 and Σ_2. For a single hole, there are two asymptotically flat regions, and its mass, equal to m, is the same independent of which region we evaluate it on. In the case of a binary system, the gravitational interaction between the holes will change the value of the individual masses. Actually, there is not an invariant measure of them in Σ_0, but such a measure does exist on Σ_1 and Σ_2. Doing the calculation yields the following result [55]

$$M_1 = m_1\left(1 + \frac{m_2}{2d}\right), \qquad M_2 = m_2\left(1 + \frac{m_1}{2d}\right), \qquad (11)$$

where $d = |\boldsymbol{R}_{12}|$. In Σ_0, we can compute the total mass of the binary system, the ADM mass of the system. We call the result M and it is given by

$$M = m_1 + m_2. \qquad (12)$$

Equations (3), (8), and (10) are the initial data. We should note that, apart from our choice of initial data (BL conformal factor and Bowen-York extrinsic curvature), there are other possible choices that can be used in the CLA scheme. Some examples of other possible data sets are the following: a Misner conformal factor with a Bowen-York extrinsic curvature with inversion symmetry through the throats; Kerr-Schild initial data [42].

The next step in the construction of the initial data is to put it in a form suitable for the CLA scheme. Before doing so, however, it is convenient to study the parameters that determine the configuration described by the data. To begin with, let us introduce the bare mass ratio

$$q = \frac{m_2}{m_1}. \qquad (13)$$

The initial configuration can then be fully specified in terms of the parameters (q, d, P). Since q and d are bare parameters, in the sense that we cannot give them a physical meaning, we are going to introduce analogous parameters, which can be given a physical interpretation. First, we introduce the mass ratio between the individual masses of the holes as computed in their respective asymptotically flat regions:

$$Q = \frac{M_2}{M_1}. \qquad (14)$$

The quantities q and Q are related through d via [44]:

$$Q = q \frac{1 + [(1 + q)/2](M/d)}{1 + [(1 + q)q/2](M/d)}, \qquad (15)$$

$$q = \frac{Q - 1}{2}\left(1 + \frac{M}{2d}\right) + \sqrt{Q + \left[\frac{Q - 1}{2}\left(1 + \frac{M}{2d}\right)\right]^2}. \qquad (16)$$

Defining a useful distance is a more difficult matter. In this paper, we use the same distance as Andrade and Price [44], which is the proper distance between the points where the marginally trapped surfaces, surrounding each individual hole, cross the X-axis (we obviously refer to crossing points closer to the opposite hole). When the initial configuration does not present a common apparent horizon, these marginally trapped surfaces are the individual components of the apparent horizon. If x_1 and x_2 stand for these crossing points, the distance we have just defined is given by $D = \int_{x_2}^{x_1} \Phi^2 dx$, which yields

$$\begin{aligned} D = \Delta x \Bigg\{ 1 &+ \frac{m_1^2}{4(X_1 - x_1)(X_1 - x_2)} \\ &+ \frac{m_2^2}{4(x_1 - X_2)(x_2 - X_2)} \Bigg\} - M_1 \ln\left(\frac{X_1 - x_1}{X_1 - x_2}\right) \\ &+ M_2 \ln\left(\frac{x_1 - X_2}{x_2 - X_2}\right), \end{aligned} \qquad (17)$$

where $\Delta x = x_1 - x_2 > 0$, and $X_1 (= R_1)$ and $X_2 (= -R_2)$ are the x-coordinate locations of holes 1 and 2, respectively, in the conformal space. In summary, we can determine our initial configuration either by specifying the set (q, d, P) or the set (Q, D, P).

The CLA scheme assumes that the black holes are sufficiently close enough, which allows us to expand the initial data in $R \gg R_1$ and $R \gg R_2$. In this sense, it is useful to choose the coordinate origin, $\boldsymbol{R} = 0$, in such a way that it coincides with the bare center of mass of the binary black hole, that is:

$$m_1\boldsymbol{R}_1 + m_2\boldsymbol{R}_2 = 0. \qquad (18)$$

We can write then $\boldsymbol{R}_1$ and $\boldsymbol{R}_2$ in terms of the separation vector $\boldsymbol{R}_{12}$ via

$$\boldsymbol{R}_1 = \chi_1 \boldsymbol{R}_{12} \qquad \boldsymbol{R}_2 = \chi_2 \boldsymbol{R}_{12}, \qquad (19)$$

where we have defined

$$\chi_1 = -\frac{q}{1 + q}, \qquad \chi_2 = \frac{1}{1 + q}. \qquad (20)$$

Then, it is natural to expand the initial data in the following dimensionless parameter ϵ

$$\epsilon = |\boldsymbol{\epsilon}| = \frac{d}{R}, \qquad \boldsymbol{\epsilon} = \frac{\boldsymbol{R}_{12}}{R}. \qquad (21)$$

A key formula for performing these expansions is the following:

$$\frac{1}{|\boldsymbol{R} - \boldsymbol{R}_A|^N} = \frac{1}{R} \sum_{\ell=0}^{\infty} C_\ell^{(N/2)}(\hat{\boldsymbol{\epsilon}} \cdot \hat{\boldsymbol{R}})(\chi_A \epsilon)^\ell, \qquad (22)$$

where we have introduced the following unit vectors

$$\hat{\boldsymbol{R}} = \frac{\boldsymbol{R}}{R}, \qquad \hat{\boldsymbol{\epsilon}} = \frac{\boldsymbol{\epsilon}}{\epsilon}, \qquad (23)$$

and where $C_\ell^{(N/2)}$ denote the Gegenbauer polynomials. These polynomials, also known as ultraspherical polyno-

mials, are a generalization of the Legendre polynomials to $(N/2 + 2)$-dimensional spaces, which are common in angular momentum theory [56,57]. For the special cases of $N = 0, 1, 2$, these polynomials reduce to Legendre polynomials and Chebyshev polynomials of type 1 and 2, respectively. We refer to Appendix A for more details on these polynomials.

We now use all these definitions and results to expand the conformal extrinsic curvature given by Eq. (8) in ϵ to arbitrary order. The result we obtain can be written as follows:

$$\hat{K}_{ij} = \frac{3}{2R^2} \sum_{\ell=0}^{\infty} \left(\frac{d}{R}\right)^{\ell+1} (\chi_1^{\ell+1} - \chi_2^{\ell+1}) \{ C_{\ell+1}^{(3/2)}[2P_{(i}\hat{R}_{j)} - (\boldsymbol{P} \cdot \hat{\boldsymbol{R}})\hat{\gamma}_{ij}] + C_{\ell+1}^{(5/2)}(\boldsymbol{P} \cdot \hat{\boldsymbol{R}})\hat{R}_i\hat{R}_j + C_\ell^{(3/2)}[(\boldsymbol{P} \cdot \hat{\boldsymbol{\epsilon}})\hat{\gamma}_{ij} - 2P_{(i}\hat{\epsilon}_{j)}]$$

$$- C_\ell^{(5/2)}[(\boldsymbol{P} \cdot \hat{\boldsymbol{\epsilon}})\hat{R}_i\hat{R}_j + 2(\boldsymbol{P} \cdot \hat{\boldsymbol{R}})\hat{R}_{(i}\hat{\epsilon}_{j)}] \} + \left(\frac{d}{R}\right)^{\ell+2} (\chi_1^{\ell+2} - \chi_2^{\ell+2}) C_\ell^{(5/2)}[(\boldsymbol{P} \cdot \hat{\boldsymbol{R}})\hat{\epsilon}_i\hat{\epsilon}_j + 2(\boldsymbol{P} \cdot \hat{\boldsymbol{\epsilon}})\hat{R}_{(i}\hat{\epsilon}_{j)}]$$

$$- \left(\frac{d}{R}\right)^{\ell+3} (\chi_1^{\ell+3} - \chi_2^{\ell+3}) C_\ell^{(5/2)}(\boldsymbol{P} \cdot \hat{\boldsymbol{\epsilon}})\hat{\epsilon}_i\hat{\epsilon}_j, \qquad (24)$$

where for simplicity we have omitted the argument of the Gegenbauer polynomials, which still is $\hat{\boldsymbol{\epsilon}} \cdot \hat{\boldsymbol{R}}$. It is worth noting that the ϵ^0 term has identically vanished due to the choice of coordinate origin, which coincides with the bare center of mass. Another interesting fact is that only combinations of the $(3/2)$- and $(5/2)$-Gegenbauer polynomials appear due to the combination of odd powers in the denominators of the extrinsic curvature.

In this paper we are going to consider terms up to $\mathcal{O}(\epsilon^3)$, which is enough to get a gravitational recoil effect and actually the dominant part of it (see, e.g. [44]). Extensions of our calculations to higher order are in principle straightforward, but we are not going to present them here. Then, up to this order of approximation we can rewrite Eq. (24) as follows:

$$\hat{K}_{ij} = \frac{9}{2} \frac{d}{R^3} \left\{ \hat{\boldsymbol{R}} \cdot \hat{\boldsymbol{\epsilon}} + \frac{1}{2} \frac{d}{R} \frac{1-q}{1+q}[5(\hat{\boldsymbol{R}} \cdot \hat{\boldsymbol{\epsilon}})^2 - 1] \right\} [(\boldsymbol{P} \cdot \hat{\boldsymbol{R}})\hat{\gamma}_{ij} - 2P_{(i}\hat{R}_{j)}]$$

$$- \frac{3}{2} \frac{d}{R^3} \left\{ 1 + 3\frac{d}{R}\frac{1-q}{1+q}\hat{\boldsymbol{R}} \cdot \hat{\boldsymbol{\epsilon}} \right\} [(\boldsymbol{P} \cdot \hat{\boldsymbol{\epsilon}})\hat{\gamma}_{ij} - 2P_{(i}\hat{\epsilon}_{j)}] - \frac{15}{2} \frac{d}{R^3} \left\{ \hat{\boldsymbol{R}} \cdot \hat{\boldsymbol{\epsilon}} + \frac{1}{2}\frac{d}{R}\frac{1-q}{1+q}[7(\hat{\boldsymbol{R}} \cdot \hat{\boldsymbol{\epsilon}})^2 - 1] \right\} (\boldsymbol{P} \cdot \hat{\boldsymbol{R}})\hat{R}_i\hat{R}_j$$

$$+ \frac{3}{2} \frac{d}{R^3} \left\{ 1 + 5\frac{d}{R}\frac{1-q}{1+q}\hat{\boldsymbol{R}} \cdot \hat{\boldsymbol{\epsilon}} \right\} [(\boldsymbol{P} \cdot \hat{\boldsymbol{\epsilon}})\hat{R}_i\hat{R}_j + 2(\boldsymbol{P} \cdot \hat{\boldsymbol{R}})\hat{R}_{(i}\hat{\epsilon}_{j)}] - \frac{3}{2}\frac{d^2}{R^4}\frac{1-q}{1+q}[(\boldsymbol{P} \cdot \hat{\boldsymbol{R}})\hat{\epsilon}_i\hat{\epsilon}_j + 2(\boldsymbol{P} \cdot \hat{\boldsymbol{\epsilon}})\hat{R}_{(i}\hat{\epsilon}_{j)}]$$

$$+ \mathcal{O}(Pd^3). \qquad (25)$$

The lowest-order contribution is of $\mathcal{O}(Pd)$ and it is the only contribution used by Khanna *et al.* [47] for grazing collisions of equal-mass black holes. The next contribution is of $\mathcal{O}(Pd^2)$ and, as far as we know, this is the first time it has been considered.

Let us now look at the conformal factor [Eq. (10)]. Using Eq. (22), we can also expand Φ in Gegenbauer polynomials to obtain

$$\Phi = 1 + \frac{M}{2R} + \sum_{\ell \geq 2}^{\infty} C_\ell^{(1/2)}(\hat{\boldsymbol{R}} \cdot \hat{\boldsymbol{\epsilon}})\epsilon^\ell (m_1\chi_1^\ell + m_2\chi_2^\ell). \quad (26)$$

It is important to recall that in solving the Hamiltonian constraint we have used a slow-motion approximation, neglecting terms of $\mathcal{O}(P^2)$. The terms we are, thus, neglecting are of $\mathcal{O}(P^2d^2)$. This expression can also be written in terms of the parameters (q, d) and M, and in terms of

Legendre polynomials. In this way we obtain

$$\Phi = 1 + \frac{M}{2R} + \sum_{\ell \geq 2}^{\infty} \phi_\ell \left(\frac{M}{R}\right)^{\ell+1} P_\ell(\hat{\boldsymbol{R}} \cdot \hat{\boldsymbol{\epsilon}}) + \mathcal{O}(P^2d^2),$$

$$(27)$$

where P_ℓ denotes the Legendre polynomials and where the coefficients ϕ_ℓ are given by

$$\phi_\ell = \frac{1}{2}\{(-1)^\ell + q^{\ell-1}\}\frac{q}{(1+q)^{\ell+1}}\left(\frac{d}{M}\right)^\ell. \quad (28)$$

The $\ell = 1$-term vanishes due to the choice of the origin of coordinates in Eq. (18). Finally, the expansion of the conformal factor up to third order in d is given by

$$\Phi = 1 + \frac{M}{2R} + \frac{1}{2} \frac{q}{(1+q)^2} \frac{Md^2}{R^3} P_2(\hat{\boldsymbol{R}} \cdot \hat{\boldsymbol{\epsilon}})$$
$$- \frac{1}{2} \frac{q(1-q)}{(1+q)^3} \frac{Md^3}{R^4} P_3(\hat{\boldsymbol{R}} \cdot \hat{\boldsymbol{\epsilon}}) + \mathcal{O}(P^2 d^2, d^4). \quad (29)$$

With this, we finish the construction of initial data to be used in the CLA scheme. To summarize, we remark that this construction is based on expansions on two different parameters: P (related to the slow-motion approximation) and d (related to the assumption that the holes are close to each other). Since P and d have dimensions, the meaning of these expansions is that terms of order d^N and/or P^M are smaller than terms of order d^{N-1} and/or P^{M-1}. As we are going to see later, these expansions will provide the leading contribution of the multipoles $\ell = 2$ and $\ell = 3$.

IV. THE CLOSE-LIMIT APPROXIMATION

The next stage in our computation is to recast the initial data just constructed into data for a perturbed Schwarzschild black hole, which is the essence of the CLA scheme. In this way we can extract initial data to be evolved by the corresponding perturbation equations. Thanks to the expansions performed in the previous section, the main task now becomes the extraction of the different multipoles from the data.

The 3-metric on the initial slice is conformally flat and hence determined by the conformal factor Φ. If we look at the lowest-order contribution [see Eq. (29)] we realize that it coincides with the 3-metric of Schwarzschild spacetime associated with the $\{t = \text{const}\}$-slicing in isotropic coordinates, being t the Schwarzschild time coordinate. However, in order to make the connection with perturbation theory, it is very convenient to reexpress the initial data in Schwarzschild coordinates:

$$ds^2 = f^{-1} dr^2 + r^2 d\Omega^2, \qquad f = 1 - \frac{2M}{r}, \quad (30)$$

where we recall that M is the total ADM mass. The transformation from isotropic coordinates to Schwarzschild coordinates is given by the following relations:

$$R = \frac{1}{4}(\sqrt{r} + \sqrt{r - 2M})^2, \qquad r = R\left(1 + \frac{M}{2R}\right)^2. \quad (31)$$

Applying this transformation to the 3-metric of our initial data we obtain:

$$ds^2 = \mathcal{F}^4(f^{-1} dr^2 + r^2 d\Omega^2), \quad (32)$$

where

$$\mathcal{F} = \frac{\Phi}{1 + \frac{M}{2R}}. \quad (33)$$

In order to construct initial data for the perturbations, evolve it, and compute from the result all the relevant physical information, in the next subsections we give a

summary of (nonrotating) black hole perturbation theory and the main tools needed for the application of the CLA scheme. Afterwards, we apply this machinery to the construction of the initial data and describe how the energy, angular momentum, and linear momentum fluxes carried away by the gravitational waves are evaluated.

A. Black hole perturbation theory

The CLA is based on the fact that, in the last stages of coalescence, the gravitational field can be modeled, to a good degree of approximation, as the gravitational field of a single perturbed black hole. Thus, perturbation theory plays a key role in our calculations and it is worth reviewing its main concepts and tools. The starting point is the assumption that the spacetime metric $g_{\mu\nu}$ can be written as: $g_{\mu\nu} = g_{\mu\nu}^{\text{Sch}} + h_{\mu\nu}$, where $g_{\mu\nu}^{\text{Sch}}$ denotes the background Schwarzschild metric and $h_{\mu\nu}$ the first-order perturbations. Then, we can take advantage of the spherical symmetry of the Schwarzschild metric to simplify the structure of the perturbations and of the equations that govern them. We can do this by expanding the perturbations in tensor spherical harmonics. It turns out that the linearized Einstein equations (in this case, around the Schwarzschild background) decouple for each harmonic. Not only this, we can distinguish between the perturbative modes with polar parity, which pick up a factor of $(-1)^l$ under parity transformations, and the ones that have axial parity, which pick up a factor of $(-1)^{l+1}$. This distinction is important because polar and axial modes also decouple.

Following this discussion, we split the metric perturbations $h_{\mu\nu}$ into polar and axial perturbations, $h_{\mu\nu} = h_{\mu\nu}^{\text{a}} + h_{\mu\nu}^{\text{p}}$. And these perturbations can be expanded in tensor spherical harmonics as

$$h_{\mu\nu}^{\text{a}} = \sum_{\ell,m} h_{\mu\nu}^{\text{a},\ell m}, \qquad h_{\mu\nu}^{\text{p}} = \sum_{\ell,m} h_{\mu\nu}^{\text{p},\ell m}, \quad (34)$$

where

$$h_{\mu\nu}^{\text{a},\ell m} = \begin{pmatrix} 0 & h_A^{\ell m} S_a^{\ell m} \\ * & H^{\ell m} S_{ab}^{\ell m} \end{pmatrix}, \quad (35)$$

$$h_{\mu\nu}^{\text{p},\ell m} = \begin{pmatrix} h_{AB}^{\ell m} Y^{\ell m} & p_A^{\ell m} Y_a^{\ell m} \\ * & r^2(K^{\ell m} Y_{ab}^{\ell m} + G^{\ell m} Z_{ab}^{\ell m}) \end{pmatrix}, \quad (36)$$

where asterisks are used to denote components that are given by the symmetry of these tensors. $Y^{\ell m}$ are the scalar spherical harmonics [see Appendix A 2 for the conventions that we use and other details]. $Y_a^{\ell m}$ and $S_a^{\ell m}$ are vector spherical harmonics and are defined (for $l \geq 1$) in terms of the scalar spherical harmonics by

$$Y_a^{\ell m} \equiv Y_{:a}^{\ell m}, \qquad S_a^{\ell m} \equiv \epsilon_a{}^b Y_b^{\ell m}. \quad (37)$$

Finally, $Y_{ab}^{\ell m}$, $Z_{ab}^{\ell m}$, and $S_{ab}^{\ell m}$ are (symmetric) tensor spherical harmonics, which can also be defined ($Z_{ab}^{\ell m}$ and $S_{ab}^{\ell m}$ only

for $l \geq 2$) in terms of the scalar spherical harmonics by

$$Y^{\ell m}_{ab} \equiv Y^{\ell m} \Omega_{ab}, \qquad Z^{\ell m}_{ab} \equiv Y^{\ell m}_{:ab} + \frac{\ell(\ell+1)}{2} Y^{\ell m} \Omega_{ab}, \tag{38}$$

$$S^{\ell m}_{ab} \equiv S^{\ell m}_{(a:b)}. \tag{39}$$

Here, the sign convention for the Levi-Civita tensor associated with the metric of the 2-sphere is: $\epsilon_{\theta\varphi} = \sin\theta$. In Appendix A 2, we give the orthogonality relations for the different harmonic objects. All perturbative quantities, scalar ($h^{\ell m}_{AB}$), vectorial ($p^{\ell m}_A$ and $q^{\ell m}_A$), and tensorial ($K^{\ell m}$, $G^{\ell m}$, and $q^{\ell m}_2$), are functions of t and r only.

The metric perturbations are in general not invariant under transformations of the mapping between the background and perturbed spacetimes, or in other words, they are in general not invariant under gauge transformations. However, for the case of a spherically symmetric background, like the Schwarzschild metric, there is a complete set of perturbative quantities that are gauge invariant. For polar modes this set can be chosen as follows

$$\tilde{h}^{\ell m}_{AB} = h^{\ell m}_{AB} - 2 v^{\ell m}_{A|B}, \tag{40}$$

$$\tilde{K}^{\ell m} = K^{\ell m} + \frac{\ell(\ell+1)}{2} G^{\ell m} - 2\frac{r^{|A}}{r} v^{\ell m}_A, \tag{41}$$

where $v^{\ell m}_A = p^{\ell m}_A - (r^2/2) G^{\ell m}_{|A}$. And for axial modes

$$\tilde{h}^{\ell m}_A = h^{\ell m}_A - \frac{1}{2} H^{\ell m}_{|A} + \frac{r_{|A}}{r} H^{\ell m}. \tag{42}$$

The equations for the metric perturbations decouple in terms of complex master functions, so that once we solve the decoupled equations for these master functions all the metric perturbations can be reconstructed from them. In the case of axial modes, it was first done by Regge and Wheeler [58], and for polar modes by Zerilli [59] and later by Moncrief [60]. These functions are made out of metric perturbations and their first derivatives and they are gauge invariant. It is also possible to express them in a covariant form. In the case of polar modes, the Zerilli-Moncrief function can be written as follows [61]

$$\Psi^{\ell m}_{\rm ZM} = \frac{r}{1+\lambda_\ell} \left\{ \tilde{K}^{\ell m} + \frac{1}{\Lambda_\ell} [r^{|A} r^{|B} \tilde{h}^{\ell m}_{AB} - rr^{|A} \tilde{K}^{\ell m}_{|A}] \right\}, \tag{43}$$

where $\lambda_\ell = (\ell+2)(\ell-1)/2$ and $\Lambda_\ell = \lambda_\ell + 3M/r$. For axial modes, instead of using the well-known Regge-Wheeler master function

$$\Psi^{\ell m}_{\rm RW} = -\frac{f}{r} r^{|A} \tilde{h}^{\ell m}_{|A}, \tag{44}$$

we are going to use the master function introduced by Cunningham, Price, and Moncrief [62], in the form used in [61,63]. The main reason for this choice is that it is simpler to evaluate the fluxes of energy, angular momen-

tum, and linear momentum. Moreover, the contributions of axial modes to these physical quantities have the same form as the one of polar modes. Nevertheless, for the sake of completeness, we provide formulae for both master functions. The Cunningham-Price-Moncrief master function can be written in covariant form as [61]

$$\Psi^{\ell m}_{\rm CPM} = \frac{r}{\lambda_\ell} \epsilon^{AB} \left(\tilde{h}^{\ell m}_{B|A} - \frac{2}{r} r_{|A} \tilde{h}^{\ell m}_B \right). \tag{45}$$

In Schwarzschild coordinates these functions take the following form (the connection with the Regge-Wheeler parametrization of the perturbations is given in Appendix B)

$$\Psi^{\ell m}_{\rm ZM} = \frac{r}{1+\lambda_\ell} \left\{ K^{\ell m} + (1+\lambda_\ell) G^{\ell m} \right.$$
$$\left. + \frac{f}{\Lambda_\ell} \left[f h^{\ell m}_{rr} - r\partial_r K^{\ell m} - \frac{2}{r}(1+\lambda_\ell) p^{\ell m}_r \right] \right\}, \tag{46}$$

$$\Psi^{\ell m}_{\rm RW} = -\frac{f}{r} \left(h^{\ell m}_r - \frac{1}{2} \partial_r H^{\ell m} + \frac{1}{r} H^{\ell m} \right), \tag{47}$$

$$\Psi^{\ell m}_{\rm CPM} = -\frac{r}{\lambda_\ell} \left\{ \dot{h}^{\ell m}_r - \partial_r h^{\ell m}_t + \frac{2}{r} h^{\ell m}_t \right\}. \tag{48}$$

These master functions obey the following wave-type equation with a potential:

$$[-\partial^2_t + \partial^2_{r_*} - V^{\rm RW/ZM}_\ell(r)] \Psi^{\ell m}_{\rm CPM/ZM} = 0, \tag{49}$$

where r_* is the so-called *tortoise* coordinate ($r_* = r + 2M \ln(r/(2M) - 1)$). The potential for the axial modes is the Regge-Wheeler potential

$$V^{\rm RW}_\ell(r) = \frac{f}{r^2} \left(\ell(\ell+1) - \frac{6M}{r} \right), \tag{50}$$

and the one for polar modes is the Zerilli potential

$$V^{\rm ZM}_\ell(r) = \frac{f}{r^2 \Lambda^2} \left[2\lambda^2_\ell \left(1 + \lambda_\ell + \frac{3M}{r} \right) + 18\frac{M^2}{r^2} \left(\lambda_\ell + \frac{M}{r} \right) \right]. \tag{51}$$

Once the different master functions have been computed we can estimate the energy and angular momentum carried out by the radiation field to infinity. We can do this by using the expressions of the energy and angular momentum fluxes at infinity obtained from the Isaacson's averaged energy-momentum tensor for gravitational waves [64,65] (see also [66,67]). In terms of the axial and polar master functions the expressions are

$$\dot{E}_{\rm GW} = \frac{1}{64\pi} \sum_{\ell \geq 2, m} \frac{(\ell+2)!}{(\ell-2)!} (|\dot{\Psi}^{\ell m}_{\rm CPM}|^2 + |\dot{\Psi}^{\ell m}_{\rm ZM}|^2), \tag{52}$$

$$\dot{L}_{\rm GW} = \frac{1}{64\pi} \sum_{\ell \geq 2, m} im \frac{(\ell+2)!}{(\ell-2)!} (\bar{\Psi}^{\ell m}_{\rm CPM} \dot{\Psi}^{\ell m}_{\rm CPM} + \bar{\Psi}^{\ell m}_{\rm ZM} \dot{\Psi}^{\ell m}_{\rm ZM}). \tag{53}$$

We can also construct the metric *waveforms* by using

$$h_+ - ih_\times = \frac{1}{2r} \sum_{\ell \geq 2, m} \sqrt{\frac{(\ell + 2)!}{(\ell - 2)!}} (\Psi_{ZM}^{\ell m} + i\Psi_{CPM}^{\ell m})_{-2}Y^{\ell m},$$
(54)

where $_{-2}Y^{\ell m}$ denotes the spherical harmonics of spin weight -2 (see, e.g. [68] and Appendix A 3 for details). In this work we are interested in studying the gravitational recoil due to the merger of unequal-mass black hole binary systems and therefore, we want to evaluate the flux of linear momentum emitted in gravitational waves. This quantity can also be computed from the Isaacson's energy-momentum tensor and can be written in terms of the metric waveforms as follows:

$$\dot{P}_{GW}^k = \frac{r^2}{16\pi} \int d\Omega \hat{r}_{obs}^k (\dot{h}_+^2 + \dot{h}_\times^2),$$
(55)

where $\hat{r}_{obs}^k$ is a unit vector that points from the source to the observer. We can then express the components of $\hat{r}_{obs}^k$ in terms of scalar spherical harmonics as

$$\hat{r}_{obs}^k = -2\sqrt{\frac{2\pi}{3}} \left(\Re(Y^{1,1}), \Im(Y^{1,1}), -\frac{Y^{1,0}}{\sqrt{2}} \right),$$
(56)

where $\Re$ and $\Im$ denote the real and imaginary parts of a complex number. By simple inspection of the linear momentum flux in Eq. (55), and taking into account the harmonic structure of the metric waveforms in Eq. (54) and of $\hat{r}_{obs}^k$ in Eq. (56), we realize that all terms in the flux contain the product of three spherical harmonic objects. Therefore, in order to obtain a practical expression for $\dot{P}_{GW}^k$ we need to use the machinery for studying coupled angular momenta common in quantum physics [56,57]. The calculation goes along the lines described in [67], and some details are given in Appendix C. The result can be written in the following form

$$\dot{P}_{GW}^x = -\frac{1}{64\pi} \sum_{\ell \geq 2, m} \frac{(\ell + 3)!}{(\ell - 2)!} \frac{1}{(\ell + 1)\sqrt{(2\ell + 3)(2\ell + 1)}} \{ \sqrt{(\ell + m + 2)(\ell + m + 1)}(\dot{\Psi}_{ZM}^{\ell m}\dot{\bar{\Psi}}_{ZM}^{\ell+1,m+1} + \dot{\Psi}_{CPM}^{\ell m}\dot{\bar{\Psi}}_{CPM}^{\ell+1,m+1}) $$
$$ - \sqrt{(\ell - m + 2)(\ell - m + 1)}(\dot{\Psi}_{ZM}^{\ell m}\dot{\bar{\Psi}}_{ZM}^{\ell+1,m-1} + \dot{\Psi}_{CPM}^{\ell m}\dot{\bar{\Psi}}_{CPM}^{\ell+1,m-1}) \},$$
(57)

$$\dot{P}_{GW}^y = \frac{i}{64\pi} \sum_{\ell \geq 2, m} \frac{(\ell + 3)!}{(\ell - 2)!} \frac{1}{(\ell + 1)\sqrt{(2\ell + 3)(2\ell + 1)}} \{ \sqrt{(\ell + m + 2)(\ell + m + 1)}(\dot{\Psi}_{ZM}^{\ell m}\dot{\bar{\Psi}}_{ZM}^{\ell+1,m+1} + \dot{\Psi}_{CPM}^{\ell m}\dot{\bar{\Psi}}_{CPM}^{\ell+1,m+1}) $$
$$ + \sqrt{(\ell - m + 2)(\ell - m + 1)}(\dot{\Psi}_{ZM}^{\ell m}\dot{\bar{\Psi}}_{ZM}^{\ell+1,m-1} + \dot{\Psi}_{CPM}^{\ell m}\dot{\bar{\Psi}}_{CPM}^{\ell+1,m-1}) \},$$
(58)

$$\dot{P}_{GW}^z = \frac{1}{32\pi} \sum_{\ell \geq 2, m} \frac{(\ell + 3)!}{(\ell - 2)!} \sqrt{\frac{(\ell + m + 1)(\ell - m + 1)}{(2\ell + 3)(2\ell + 1)(\ell + 1)^2}} (\dot{\Psi}_{ZM}^{\ell m}\dot{\bar{\Psi}}_{ZM}^{\ell+1,m} + \dot{\Psi}_{CPM}^{\ell m}\dot{\bar{\Psi}}_{CPM}^{\ell+1,m}).$$
(59)

In conclusion, all we need to extract relevant physical information is the master functions. In the next subsections, we extract initial data for these master functions.

B. Relation between ADM variables and metric perturbation

In Sec. III, we constructed initial data for a binary black hole system in coalescence. The procedure used for this construction was based on the $3 + 1$ ADM formalism [69] and, hence, the initial data is given in terms of ADM variables [Eqs. (3), (25), and (29)]. Then, in order to build initial data for the evolution of the master functions, we need to first find the relation between the ADM variables and the metric perturbations (see, e.g. [70]). This means that we need to use the relations between the components of the 3-metric γ_{ij} and the metric perturbations, and also the relations between the metric perturbations and their first derivatives and the components of the extrinsic curvature K_{ij}. For the former, we use the fact that the components of the 3-metric are the spatial components of the orthogonal projection operator on the hypersurfaces of the spacetime slicing, described by a normal n_μ:

$$\gamma_{\mu\nu} = g_{\mu\nu} + n_\mu n_\nu.$$
(60)

Then, the different modes of the harmonically decomposed 3-metric are related to the metric perturbations via

$$\gamma_{tt}^{\ell m} = -f\delta^{0,0},$$
(61)

$$\gamma_{tr}^{\ell m} = h_{tr}^{\ell m}Y^{\ell m},$$
(62)

$$\gamma_{ta}^{\ell m} = p_t^{\ell m}Y_a^{\ell m} + h_t^{\ell m}S_a^{\ell m},$$
(63)

$$\gamma_{rr}^{\ell m} = f^{-1}\delta^{0,0} + h_{rr}^{\ell m}Y^{\ell m},$$
(64)

$$\gamma_{ra}^{\ell m} = p_r^{\ell m}Y_a^{\ell m} + h_r^{\ell m}S_a^{\ell m},$$
(65)

$$\gamma_{ab}^{\ell m} = r^2\Omega_{ab}\delta^{0,0} + r^2(K^{\ell m}Y_{ab}^{\ell m} + G^{\ell m}Z_{ab}^{\ell m}) + H^{\ell m}S_{ab}^{\ell m}.$$
(66)

The first three equations are related to the choice of slicing, that is, to the choice of shift vector β^i and lapse α. Actually, the lapse and shift at first order are given by

$$\alpha^2 = f(1 - fh^{tt}) = f - h_{tt} + \mathcal{O}(h^2), \qquad (67)$$

$$\beta^i = h_t^i + \mathcal{O}(h^2). \qquad (68)$$

The relation between the extrinsic curvature and the metric perturbations can be found through the relation between the 3-metric and the extrinsic curvature

$$K_{\mu\nu} = -\tfrac{1}{2}\mathcal{L}_{\mathbf{n}}\gamma_{\mu\nu}, \qquad (69)$$

where the symbol $\mathcal{L}$ denotes Lie differentiation, and Eq. (60) between the 3-metric and the spacetime metric. In this way, we find that the different modes of the harmonically decomposed extrinsic curvature are related to the metric perturbations by the following expressions:

$$K_{rr}^{\ell m} = \frac{1}{2\sqrt{f}}\left[\dot{h}_{rr}^{\ell m} - 2h_{tr}^{\ell m\prime} - \frac{f'}{f}h_{tr}^{\ell m}\right]Y^{\ell m}, \qquad (70)$$

$$K_{ra}^{\ell m} = \frac{1}{2\sqrt{f}}\left\{\left[\dot{p}_r^{\ell m} - p_t^{\ell m\prime} + \frac{2}{r}p_t^{\ell m} - h_{tr}^{\ell m}\right]Y_a^{\ell m} \right.$$
$$\left. + \left[\dot{h}_r^{\ell m} - h_t^{\ell m\prime} + \frac{2}{r}h_t^{\ell m}\right]S_a^{\ell m}\right\}, \qquad (71)$$

$$K_{ab}^{\ell m} = \frac{r^2}{2\sqrt{f}}\left\{\left[\dot{K}^{\ell m} + \frac{\ell(\ell+1)}{r^2}p_t^{\ell m} - \frac{2f}{r}h_{tr}^{\ell m}\right]Y_{ab}^{\ell m} \right.$$
$$\left. + \left[\dot{G}^{\ell m} - \frac{2}{r^2}p_t^{\ell m}\right]Z_{ab}^{\ell m} + \frac{1}{r^2}[\dot{H}^{\ell m} - 2h_t^{\ell m}]S_{ab}^{\ell m}\right\}, \qquad (72)$$

where the dots and primes denote partial differentiation with respect to time t and radial coordinate r, respectively.

C. Initial data for the metric perturbations

Before computing initial data for the master functions, we must find data for the metric perturbations, that is, find $(h_{\mu\nu}, \dot{h}_{\mu\nu})$, in the parametrization given in Eqs. (35) and (36) on the initial slice $t = t_o$. To begin with, since our 3-metric is conformally flat, the following metric perturbations vanish on the initial slide:

$$p_r^{\ell m} = G^{\ell m} = 0, \qquad h_r^{\ell m} = H^{\ell m} = 0. \qquad (73)$$

We have also seen that the conformal factor, the physical and the conformal extrinsic curvatures can be formally expanded in powers of d and P as follows

$$\Phi = \Phi_{(0)} + \Phi_{(2)}d^2 + \Phi_{(3)}d^3 + \mathcal{O}(P^2d^2, d^4), \qquad (74)$$

$$\hat{K}_{ij} = Pd\hat{K}_{(1)ij} + Pd^2\hat{K}_{(2)ij} + \mathcal{O}(Pd^3), \qquad (75)$$

where $\hat{K}_{(1)ij}$ and $\hat{K}_{(2)ij}$ are the coefficients of the terms of order Pd and Pd^2, respectively, in the expansion of $\hat{K}_{ij}$.

Then, the physical extrinsic curvature, K_{ij}, given by Eq. (3), can be formally expanded in the form

$$K_{ij} = \Phi_{(0)}^{-2}(Pd\hat{K}_{(1)ij} + Pd^2\hat{K}_{(2)ij}) + \mathcal{O}(Pd^3), \qquad (76)$$

which means that in order to obtain the physical extrinsic curvature up to $\mathcal{O}(Pd^2)$ we only need the zeroth order piece of the conformal factor. The explicit expressions of the coefficients of these expansions are given by Eqs. (3), (25), and (29).

With this in mind, we are going to extract the remaining modes of the initial data. To that end, we use the expression of the separation vector $\hat{\boldsymbol{\epsilon}}$ in spherical coordinates, namely

$$\hat{\epsilon}^i = \left(\sin\theta\cos\varphi, \frac{\cos\theta\cos\varphi}{R}, -\frac{\sin\varphi}{R\cos\theta}\right). \qquad (77)$$

Then, the nonzero components of the 3-metric on the initial slice are given by

$$\gamma_{rr} = f^{-1}\left[1 + 2\frac{q}{(1+q)^2}\frac{Md^2}{r^3}\frac{1}{\sigma^5}P_2(\xi) \right.$$
$$\left. - 2\frac{q(1-q)}{(1+q)^3}\frac{Md^3}{r^4}\frac{1}{\sigma^7}P_3(\xi)\right] + \mathcal{O}(P^2d^2, d^4), \quad (78)$$

$$\gamma_{ab} = r^2\Omega_{ab}\left[1 + 2\frac{q}{(1+q)^2}\frac{Md^2}{r^3}\frac{1}{\sigma^5}P_2(\xi) \right.$$
$$\left. - 2\frac{q(1-q)}{(1+q)^3}\frac{Md^3}{r^4}\frac{1}{\sigma^7}P_3(\xi)\right] + \mathcal{O}(P^2d^2, d^4), \quad (79)$$

where we have introduced the following definitions

$$\xi = \sin\theta\cos\varphi, \qquad \sigma = \frac{1+\sqrt{f}}{2}. \qquad (80)$$

We can now rewrite the 3-metric in terms of spherical harmonics as follows

$$\gamma_{rr} = f^{-1}\{1 - 2\sqrt{\frac{\pi}{5}}\frac{q}{(1+q)^2}\frac{Md^2}{r^3}\frac{1}{\sigma^5}[Y^{2,0} - \sqrt{6}\Re(Y^{2,2})]$$
$$- 2\sqrt{\frac{\pi}{7}}\frac{q(1-q)}{(1+q)^3}\frac{Md^3}{r^4}\frac{1}{\sigma^7}[\sqrt{3}\Re(Y^{3,1}) - \sqrt{5}\Re(Y^{3,3})]\}$$
$$+ \mathcal{O}(P^2d^2, d^4), \qquad (81)$$

$$\gamma_{ab} = r^2\Omega_{ab} - 2\sqrt{\frac{\pi}{5}}\frac{q}{(1+q)^2}\frac{Md^2}{r}\frac{1}{\sigma^5}[Y_{ab}^{2,0} - \sqrt{6}\Re(Y_{ab}^{2,2})]$$
$$- 2\sqrt{\frac{\pi}{7}}\frac{q(1-q)}{(1+q)^3}\frac{Md^3}{r^2}\frac{1}{\sigma^7}[\sqrt{3}\Re(Y_{ab}^{3,1}) - \sqrt{5}\Re(Y_{ab}^{3,3})]$$
$$+ \mathcal{O}(P^2d^2, d^4). \qquad (82)$$

In order to repeat this procedure with the extrinsic curvature, we first need to compute the components of the conformal extrinsic curvature with the separation vector $\hat{\boldsymbol{\epsilon}}$ of Eq. (77). The components of the conformal extrinsic curvature are given by

$$\hat{K}_{RR} = 3\frac{Pd}{R^3}\sin^2\theta\sin(2\varphi) - 3\frac{1-q}{1+q}\frac{Pd^2}{R^4}$$
$$\times \sin\varphi\sin\theta(5\sin^2\theta\cos^2\varphi - 2) + \mathcal{O}(Pd^3), \quad (83)$$

$$\hat{K}_{R\theta} = \frac{3}{4}\frac{1-q}{1+q}\frac{Pd^2}{R^3}\cos\theta\sin\varphi(5\sin^2\theta\cos^2\varphi + 3)$$
$$+ \mathcal{O}(Pd^3), \quad (84)$$

$$\hat{K}_{R\varphi} = 3\frac{Pd}{R^2}\sin^2\theta + \frac{3}{4}\frac{1-q}{1+q}\frac{Pd^2}{R^3}$$
$$\times \sin\theta\cos\varphi[\sin^2\theta(5\cos^2\varphi - 14) + 3]$$
$$+ \mathcal{O}(Pd^3), \quad (85)$$

$$\hat{K}_{\theta\theta} = \frac{3}{8}\frac{Pd}{R}\sin(2\varphi)[\cos(2\theta) - 5] - \frac{3}{4}\frac{1-q}{1+q}\frac{Pd^2}{R^2}$$
$$\times \sin\theta\sin\varphi[5\cos^2\varphi(\cos^2\theta - 3) + 3] + \mathcal{O}(Pd^3), \quad (86)$$

$$\hat{K}_{\theta\varphi} = -\frac{3}{4}\frac{Pd}{R}\sin(2\theta)\cos(2\varphi) + \frac{3}{2}\frac{1-q}{1+q}$$
$$\times \frac{Pd^2}{R^2}\sin^2\theta\cos\theta\cos\varphi(5\cos^2\varphi - 2) + \mathcal{O}(Pd^3), \quad (87)$$

$$\hat{K}_{\varphi\varphi} = \frac{3}{8}\frac{Pd}{R}\sin^2\theta\sin(2\varphi)[1 + 3\cos(2\theta)] + \frac{15}{4}\frac{1-q}{1+q}$$
$$\times \frac{Pd^2}{R^2}\sin^3\theta\sin\varphi[\cos^2\varphi(3\sin^2\theta - 2) - 1]$$
$$+ \mathcal{O}(Pd^3). \quad (88)$$

Here we have checked that the terms of $\mathcal{O}(Pd)$ agree with those in [47] (up to a typo in their value of the $\{\theta, \varphi\}$ component). The next step is the calculation of the physical extrinsic curvature in terms of spherical harmonics and Schwarzschild coordinates. This quantity is given by

$$K_{rr} = 4\sqrt{\frac{6\pi}{5}}\frac{Pd}{r^3}\frac{1}{f}\Im(Y^{2,2}) - 2\sqrt{\frac{3\pi}{7}}\frac{1-q}{1+q}\frac{Pd^2}{r^4}\frac{1}{f\sigma^2}$$
$$\times [\sqrt{14}\Im(Y^{1,1}) + \Im(Y^{3,1}) - \sqrt{15}\Im(Y^{3,3})]$$
$$+ \mathcal{O}(Pd^3), \quad (89)$$

$$K_{ra} = 2\sqrt{3\pi}\frac{Pd}{r^2}\frac{1}{\sqrt{f}}S_a^{1,0} + \frac{1}{2}\sqrt{\frac{\pi}{21}}\frac{1-q}{1+q}\frac{Pd^2}{r^3}\frac{1}{\sqrt{f}\sigma^2}$$
$$\times \left[6\sqrt{14}\Im(Y_a^{1,1}) + 16\sqrt{\frac{14}{5}}\Re(S_a^{2,1}) + \Im(Y_a^{3,1})\right.$$
$$\left. - \sqrt{15}\Im(Y_a^{3,3})\right] + \mathcal{O}(Pd^3), \quad (90)$$

$$K_{ab} = -\sqrt{\frac{6\pi}{5}}\frac{Pd}{r}[2\Im(Y_{ab}^{2,2}) + \Im(Z_{ab}^{2,2})] + \frac{1}{2}\sqrt{\frac{\pi}{21}}\frac{1-q}{1+q}\frac{Pd^2}{r^2}$$
$$\times \frac{1}{\sigma^2}\left\{6\sqrt{14}\Im(Y_{ab}^{1,1}) - 8\sqrt{\frac{14}{5}}\Re(S_{ab}^{2,1}) + 6\Im(Y_{ab}^{3,1})\right.$$
$$+ \Im(Z_{ab}^{3,1}) - \sqrt{15}[6\Im(Y_{ab}^{3,3}) + \Re(Z_{ab}^{3,3})]\right\} + \mathcal{O}(Pd^3). \quad (91)$$

Equations (81), (82), and (89)–(91) give the complete harmonic decomposition of the initial data (γ_{ij}, K_{ij}). We must now extract the initial values of the metric perturbations and their time derivative by comparing these expressions with Eqs. (64)–(66) and (70)–(72). To simplify notation, we now drop the truncation error in all equations, since it has already been given in the main expansions. Comparison of Eqs. (81) and (82) with Eqs. (64)–(66) yields the nonvanishing initial metric perturbations, namely

$$K^{2,0} = fh_{rr}^{2,0} = -2\sqrt{\frac{\pi}{5}}\frac{q}{(1+q)^2}, \quad (92)$$

$$K^{2,\pm 2} = fh_{rr}^{2,\pm 2} = \sqrt{\frac{6\pi}{5}}\frac{q}{(1+q)^2}\frac{Md^2}{r^3}\frac{1}{\sigma^5}, \quad (93)$$

$$K^{3,\pm 1} = fh_{rr}^{3,\pm 1} = -\sqrt{\frac{3\pi}{7}}\frac{q(1-q)}{(1+q)^3}\frac{Md^3}{r^4}\frac{1}{\sigma^7}, \quad (94)$$

$$K^{3,\pm 3} = fh_{rr}^{3,\pm 3} = \sqrt{\frac{5\pi}{7}}\frac{q(1-q)}{(1+q)^3}\frac{Md^3}{r^4}\frac{1}{\sigma^7}. \quad (95)$$

As we can see, all the axial metric perturbations initially vanish. Now, in order to obtain the initial values of the time derivative of the metric perturbations, we must compare Eqs. (89)–(91) with Eqs. (70)–(72). It is important to realize that in Eqs. (70)–(72) there are terms that are associated with the gauge freedom of choosing the slicing, more specifically, terms associated with components of the shift vector [see Eq. (68)]. Moreover, there is no unique way of assigning values to the different time derivatives of the metric perturbations and the metric perturbations themselves. This reflects the fact that the values of the metric perturbations are gauge dependent, since in general the components of the metric perturbations (and their time derivatives) are not gauge invariant. Keeping this in mind, we have assigned the following initial values to the time derivatives of the metric perturbations: the nonvanishing polar modes are

$$\dot{h}_{rr}^{2,\pm 2} = \mp 24i\sqrt{\frac{\pi}{30}}\frac{Pd}{r^3}\frac{1}{\sqrt{f}}, \quad (96)$$

$$\dot{h}_{rr}^{3,\pm1} = \pm 2i\sqrt{\frac{3\pi}{7}}\frac{1-q}{1+q}\frac{Pd^2}{r^4}\frac{1}{\sqrt{f}\sigma^2}, \qquad (97)$$

$$\dot{h}_{rr}^{3,\pm3} = \mp 6i\sqrt{\frac{5\pi}{7}}\frac{1-q}{1+q}\frac{Pd^2}{r^4}\frac{1}{\sqrt{f}\sigma^2}, \qquad (98)$$

$$\dot{p}_{r}^{3,\pm1} = \mp \frac{i}{2}\sqrt{\frac{\pi}{21}}\frac{1-q}{1+q}\frac{Pd^2}{r^3}\frac{1}{\sigma^2}, \qquad (99)$$

$$\dot{p}_{r}^{3,\pm3} = \pm \frac{i}{2}\sqrt{\frac{5\pi}{7}}\frac{1-q}{1+q}\frac{Pd^2}{r^3}\frac{1}{\sigma^2}, \qquad (100)$$

$$\dot{G}^{2,\pm2} = \pm i\sqrt{\frac{6\pi}{5}}\frac{Pd}{r^3}\sqrt{f}, \qquad (101)$$

$$\dot{K}^{2,\pm2} = \pm 2i\sqrt{\frac{6\pi}{5}}\frac{Pd}{r^3}\sqrt{f}, \qquad (102)$$

$$\dot{G}^{3,\pm1} = \mp \frac{i}{2}\sqrt{\frac{\pi}{21}}\frac{1-q}{1+q}\frac{Pd^2}{r^4}\frac{\sqrt{f}}{\sigma^2}, \qquad (103)$$

$$\dot{K}^{3,\pm1} = \mp i\sqrt{\frac{3\pi}{7}}\frac{1-q}{1+q}\frac{Pd^2}{r^4}\frac{\sqrt{f}}{\sigma^2}, \qquad (104)$$

$$\dot{G}^{3,\pm3} = \pm \frac{i}{2}\sqrt{\frac{5\pi}{7}}\frac{1-q}{1+q}\frac{Pd^2}{r^4}\frac{\sqrt{f}}{\sigma^2}, \qquad (105)$$

$$\dot{K}^{3,\pm3} = \pm 3i\sqrt{\frac{5\pi}{7}}\frac{1-q}{1+q}\frac{Pd^2}{r^4}\frac{\sqrt{f}}{\sigma^2}; \qquad (106)$$

and the axial ones are

$$\dot{h}_{r}^{1,0} = 4\sqrt{3\pi}\frac{Pd}{r^2}, \qquad (107)$$

$$\dot{h}_{r}^{2,\pm1} = 8\sqrt{\frac{2\pi}{15}}\frac{1-q}{1+q}\frac{Pd^2}{r^3}\frac{1}{\sigma^2}, \qquad (108)$$

$$\dot{H}^{2,\pm1} = -4\sqrt{\frac{2\pi}{15}}\frac{1-q}{1+q}\frac{Pd^2}{r^2}\frac{\sqrt{f}}{\sigma^2}. \qquad (109)$$

By using the correspondence between our parametrization of the metric perturbations and that of Regge-Wheeler [Eqs. (B1)–(B5) in Appendix B] we have checked that up to $\mathcal{O}(d^2)$ and $\mathcal{O}(Pd)$ our expressions agree with those found in [47] (up to a typo in their $\dot{h}_{r}^{1,0}$). We have decided to assign values to the time derivatives of the metric perturbations and the metric perturbations themselves by the following usual convention: all modes with $\ell = 1$ are assigned to metric perturbations associated with the shift

vector. These perturbations represent either translations or rotations of the observers associated with the normal to the initial slice with respect to our coordinate system. In our case, these perturbations are given through the following relationships

$$fh_{tr}^{1,\pm1'} + \frac{f'}{2}h_{tr}^{1,\pm1} = \mp i\sqrt{6\pi}\frac{1-q}{1+q}\frac{Pd^2}{r^4}\frac{\sqrt{f}}{\sigma^2}, \qquad (110)$$

$$p_{t}^{1,\pm1'} - \frac{2}{r}p_{t}^{1,\pm1} + h_{tr}^{1,\pm1} = \pm i\sqrt{6\pi}\frac{Pd^2}{r^3}\frac{1-q}{1+q}\frac{1}{\sigma^2}, \qquad (111)$$

$$p_{t}^{1,\pm1} - rfh_{tr}^{1,\pm1} = \mp i\sqrt{\frac{3\pi}{2}}\frac{1-q}{1+q}\frac{Pd^2}{r^2}\frac{\sqrt{f}}{\sigma^2}. \qquad (112)$$

Here, two comments are in order. First, one can see that these equations are consistent in the sense that the derivative of Eq. (112) with respect to r can be reduced to a trivial identity by using Eqs. (110) and (111). Second, from these equations we can immediately see that the shift vector is different from zero [see Eq. (68)]. A nonzero shift could in principle be a problem if we wanted to place observers at constant r (in the wave zone), evaluate the linear momentum flux, and then infer a recoil velocity of the final black hole after the merger. If we were to do this, the measured velocity would have a component due to the motion of the observers with respect to the position of the final black hole, as described by the shift vector. This contribution would then have to be subtracted, but it can be seen that the shift vector decays quite fast as r becomes large and, hence, this effect would be negligible.

D. Initial data for the master functions

Using the initial data for the metric perturbations [Eqs. (92)–(109)] in the master functions [Eqs. (46)–(48)], we can compute initial data for them: $(\Psi_{\text{ZM}}^{\ell m}, \dot{\Psi}_{\text{ZM}}^{\ell m})$, $(\Psi_{\text{RW}}^{\ell m}, \dot{\Psi}_{\text{RW}}^{\ell m})$, and $(\Psi_{\text{CPM}}^{\ell m}, \dot{\Psi}_{\text{CPM}}^{\ell m})$ on the initial slice $t = t_o$.

The results for the Regge-Wheeler master function are:

$$\Psi_{\text{RW}}^{\ell m} = 0, \qquad (113)$$

$$\dot{\Psi}_{\text{RW}}^{2,\pm1} = -2\sqrt{\frac{2\pi}{15}}\frac{1-q}{1+q}\frac{Pd^2}{r^4}\frac{\sqrt{f}(1-\sqrt{f})}{\sigma^2}(7\sigma-3), \qquad (114)$$

and for the Cunningham-Price-Moncrief master function are

$$\Psi_{\text{CPM}}^{2,\pm1} = -\frac{4}{3}\frac{\sqrt{6\pi}}{5}\frac{1-q}{1+q}\frac{Pd^2}{r^2}\frac{1}{\sigma^2}, \qquad (115)$$

$$\dot{\Psi}_{\text{CPM}}^{\ell m} = 0. \qquad (116)$$

In the same way, the nonvanishing initial data for the Zerilli-Moncrief master functions is given by

$$\Psi_{\text{ZM}}^{2,0} = -\frac{2}{3}\sqrt{\frac{\pi}{5}}\frac{q}{(1+q)^2}\frac{Md^2}{r^2}\frac{1+5\sigma}{\Lambda_2\sigma^5},$$ (117)

$$\Psi_{\text{ZM}}^{2,\pm2} = \sqrt{\frac{2\pi}{15}}\frac{q}{(1+q)^2}\frac{Md^2}{r^2}\frac{1+5\sigma}{\Lambda_2\sigma^5},$$ (118)

$$\Psi_{\text{ZM}}^{3,\pm1} = -\frac{1}{2}\sqrt{\frac{\pi}{21}}\frac{q(1-q)}{(1+q)^3}\frac{Md^3}{r^3}\frac{3+7\sigma}{\Lambda_3\sigma^7},$$ (119)

$$\Psi_{\text{ZM}}^{3,\pm3} = \frac{1}{6}\sqrt{\frac{5\pi}{7}}\frac{q(1-q)}{(1+q)^3}\frac{Md^3}{r^3}\frac{3+7\sigma}{\Lambda_3\sigma^7},$$ (120)

$$\dot\Psi_{\text{ZM}}^{2,\pm2} = \pm i\sqrt{\frac{6\pi}{5}}\frac{Pd}{r^2}\frac{\sqrt{f}}{\Lambda_2}\left(4+\frac{3M}{r}\right),$$ (121)

$$\dot\Psi_{\text{ZM}}^{3,\pm1} = \mp\frac{i}{2}\sqrt{\frac{\pi}{21}}\frac{1-q}{1+q}\frac{Pd^2}{r^3}\frac{\sqrt{f}}{\Lambda_3\sigma^2}\left[10\sigma+(1+3\sigma)\frac{M}{r}\right],$$ (122)

$$\dot\Psi_{\text{ZM}}^{3,\pm3} = \pm\frac{i}{2}\sqrt{\frac{5\pi}{7}}\frac{1-q}{1+q}\frac{Pd^2}{r^3}\frac{\sqrt{f}}{\Lambda_3\sigma^2}\left[10\sigma+(1+3\sigma)\frac{M}{r}\right].$$ (123)

Note that the master equations do not have the same uncontrolled remainders as their derivatives, since they come from different components of the initial data. In the case of unboosted head-on collisions [44], the initial data scales in powers of d^N. Therefore, one only needs to perform one single numerical evolution of the master functions for some reference value of $d = d^\star$, and the results for any other value of d can be found using the scaling relation. For non-time-symmetric data, such as for quasicircular or boosted sets, such scaling does not exist. In our case, for example, although $\Psi_{\text{ZM}}^{\ell m}$ still scales as d^N, its time derivative $\dot\Psi_{\text{ZM}}^{\ell m}$ scales as Pd^N. Therefore, the master functions themselves are not straightforwardly scalable and several runs with different values of the initial parameters must be performed.

V. RESULTS FROM THE CLA

In this section, we evolve the master functions with the initial data obtained in the previous sections in the CLA scheme and report the results for the main physical quantities, in particular, for the gravitational recoil velocities. We first need to choose appropriately the parameters that completely determine the initial data, such that it describes a binary black hole system merging from a quasicircular orbit (subsection V A). Then, in subsection V B, we use a numerical code to evolve the different master equations [Eqs. (49)] and compute the relevant physical quantities.

We discuss the results and compare with previous ones in the literature when possible.

A. Determining the parameters of the initial data

Our initial data depends on the following parameters:
(i)   The total (ADM) mass of the system, M;
(ii) The mass ratio, where one can use either the bare mass ratio q or the physical one Q, related by Eqs. (15) and (16).
(iii) The initial separation, where again one can use the bare separation d or the physical one D, related by Eq. (17);
(iv) The linear momentum parameter P of each individual hole.

Within the family of initial data spanned by these four parameters, we need to single out the subset that corresponds to configurations in quasicircular orbital motion. In numerical relativity this is done by looking at the minimum in the binding energy of the system with respect to the distance, while keeping the total ADM angular momentum constant (see, e.g. [52]). We here follow the same procedure without using the slow-motion approximation. The binding energy that we minimize is

$$E_b = \mathcal{M}_{\text{ADM}} - \mathcal{M}_1 - \mathcal{M}_2,$$ (124)

where $\mathcal{M}_{\text{ADM}}$ is the total ADM mass and it is computed in the asymptotically flat region containing the two holes (Σ_0). This mass is given by (see, e.g. [71])

$$\mathcal{M}_{\text{ADM}} = M + \frac{5P^2}{8\mu},$$ (125)

where M is given in Eq. (12) and μ is the reduced bare mass, i.e. $\mu = m_1 m_2/M$. Moreover, in Eq. (124), $\mathcal{M}_1$ and $\mathcal{M}_2$ denote the masses computed in the asymptotically flat regions Σ_1 and Σ_2. These masses are given by (see, e.g. [71])

$$\mathcal{M}_\Lambda = M_\Lambda + \frac{P^2}{8m_\Lambda} \qquad (\Lambda = 1,2),$$ (126)

where M_Λ is given in Eq. (11). Then, the binding energy can be written in the following form

$$E_b = -\frac{m_1 m_2}{d} + \frac{J^2}{2\mu d^2},$$ (127)

where J is the ADM angular momentum, given by $J = Pd$. This binding energy is formally the same as the one corresponding to a binary system in Newtonian gravity. One can then minimize this binding energy with respect to d, while keeping J fixed, to obtain the condition for quasicircular motion (note that in our context there is no such thing as an ISCO)

$$d = \frac{J^2}{\mu^2 M}.$$ (128)

In the same way, one can calculate the associated orbital frequency of such orbital motion by differentiating the binding energy with respect to J, while keeping d fixed. The result is

$$\Omega = \frac{J}{\mu d^2}. \tag{129}$$

From Eq. (128) we can write the linear momentum P is terms of the other parameters of our initial data as

$$P = \mu \sqrt{\frac{M}{d}}. \tag{130}$$

The binding energy and other quantities derived from it have a Newtonian form because of the particular type of initial data that we are using: a conformally flat 3-metric with a Bowen-York extrinsic curvature and a Brill-Lindquist conformal factor. The PN metric produced by a binary system differs from conformal flatness at $\mathcal{O}(v^4)$ (see [72,73] for the argument in the case of time-symmetric initial data), and, hence, the binding energy used above differs from the PN binding energy at that order. Note, however, that although the binding energy, linear and angular momentum used here have a Newtonian form, they are not strictly Newtonian. This is mainly because the distance parameter d is not the physical distance D, which is related to the parameter d via Eq. (17).

Adopting Eq. (130) for the linear momentum parameter in our initial data and leaving the total mass M fixed (which defines a system of units), we reduce our initial parameter space to a 2-dimensional one. The final parameter space can be parametrized either by the bare quantities (q, d) or by the physical quantities (Q, D). The range of q, or Q, is the obvious one, i.e. [0, 1], while the range for the bare distance parameter d is $[d_{\min}, d_{\text{CLA}}]$, where d_{CLA} is an estimate of the maximum distance for which the CLA is expected to be valid. For the case of equal-mass head-on collisions, it has been shown [36], by comparing with second-order calculations and with fully numerical relativistic simulations, that $d_{\text{CLA}} \sim 1.7M$, which roughly corresponds to $D_{\text{CLA}} \sim 4M$. On the other hand, in principle $d_{\min}$ could be just zero, however, if we adopt the prescription (130) for the linear momentum parameter, then we are limited by the slow-motion approximation that we are using, which means that $d_{\min}$ should be bigger than $qM/(1 + q)^2$. Finally, we should remark that the CLA also is expected to fail in the point-particle limit [74], but, as we will see, the recoil is very small when $Q \ll 1$.

In order to study the gravitational recoil in the CLA scheme, we are going to evaluate the recoil velocity for a representative number of (physical) mass ratios for a given fixed physical distance D. In particular, we study the cases $D = 3, 3.5, 4M$ and instead of using Q we use the physical symmetric mass ratio

$$\eta = \frac{M_1 M_2}{(M_1 + M_2)^2} = \frac{Q}{(1 + Q)^2}. \tag{131}$$

The inverse relation is given by

$$Q = \frac{1}{2\eta}(1 - \sqrt{1 - 4\eta}) - 1. \tag{132}$$

However, the parameters that appear in our expressions for the initial data are the bare ones. Then, in order to obtain a plot of the recoil velocity in terms of the physical mass ratio, we need to translate from the set (Q, D) to (q, d). This, however, is not a trivial calculation because the definition of D [Eq. (17)] is quite intricate, involving x_1 and x_2. These numbers are the values of the coordinate x in the conformal flat space of the intersections of the extremal surfaces (marginally trapped surfaces or apparent horizons depending on the parameters of each particular configuration) surrounding each individual hole with the X-axis. The translation has to be done numerically through the following iteration scheme in which the physical distance D is kept fixed:

(1) Given a value of η we pick an initial guess for the bare distance, say d_*.

(2) By solving the equations that determine the extremal surfaces surrounding each individual holes (they are given in Appendix D) we find some intersection points x_1^* and x_2^*. This requires another iteration, since we do not know *a priori* where these surfaces are located. What we do is to start, for each individual hole, with an initial guess for the intersection of the extremal surface at the other end of the X-axis (the intersection more distant from the other hole) and integrate the corresponding ordinary differential equations (ODEs) by using an extrapolation Bulirsch-Stoer scheme [75–77]. Then we study whether the integration ends far away from the X-axis or converges towards it. We repeat the iteration until we find the intersection points x_1^* and x_2^* with enough accuracy.

(3) Using Eq. (17) we compute the physical distance associated with these values of the intersection points and (q_*, d_*) [where q_* is computed in terms of η and d_* using expressions (16) and (132)], D_*.

We compare D_* and D and stop the iteration if the absolute difference between them is smaller than $10^{-4}M$. Otherwise, we go back to point (i) changing the ansatz depending on whether D_* is bigger or smaller than D.

We have carried out this iteration for 101 values of η. The coordinate distance (in the conformally related flat space) from the holes to the intersection points of the extremal surfaces is shown in Fig. 2. Here, we observe how these distances move from equal values (top right) to the values corresponding to the point-particle limit, $M_2 \to m_2 \to 0$ (top left). The bare distance as a function of η is shown in Fig. 3 for the three values of fixed proper separation.
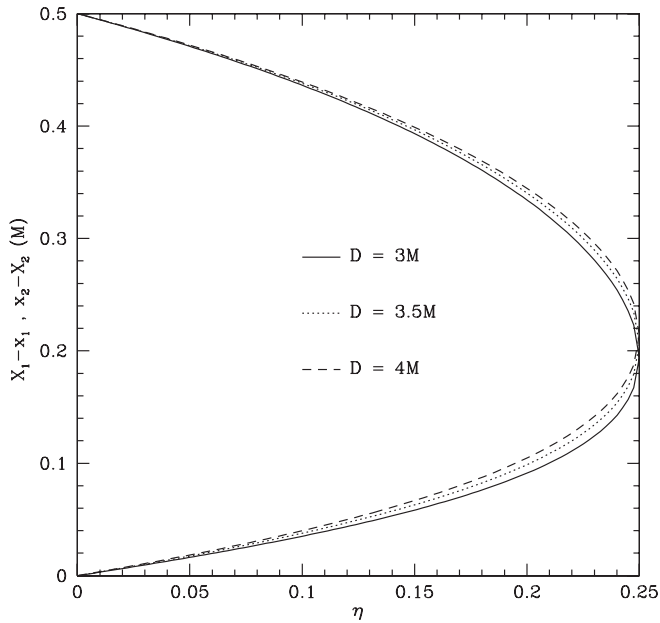
FIG. 2. Plot of the coordinate distance between the holes and the intersection points of the extremal surfaces with the *X*-axis in terms of the symmetric mass ratio η for three values of the physical distance: $D = 3, 3.5, 4M$.
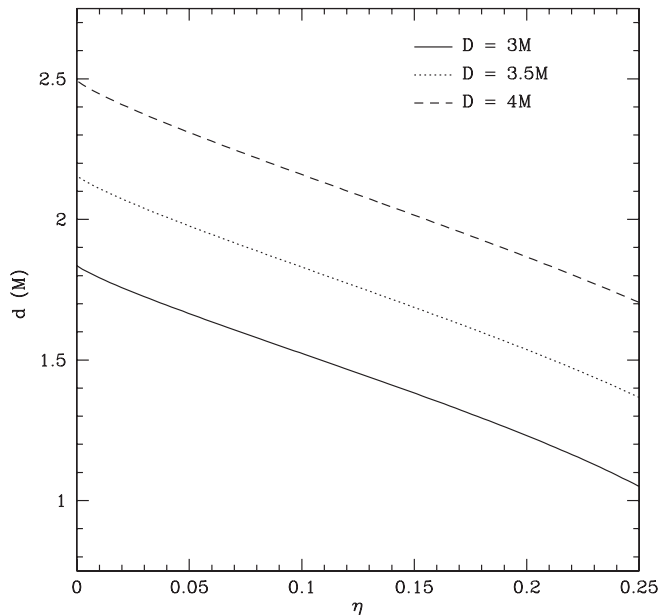

FIG. 3. Plot of the bare distance d in terms of the symmetric mass ratio η for three values of the physical distance: $D = 3, 3.5, 4M$.

B. Results from the numerical evolution of the master equations

We now have initial data for the master equations and also a method to prescribe the initial data parameters in a meaningful way. Then, the next step is to evolve the master equations [Eq. (49)]. In this paper we use a numerical code,

based on finite element methods, that was developed in [78] for calculations of the gravitational radiation emitted by a point particle orbiting a nonrotating black hole. This method is based on linear elements and hence it has a second-order convergence rate with respect to the spatial resolution. The time-evolution algorithms that it uses are second order and unconditionally stable, since they are based on implicit methods. Apart from the tests of the numerical code carried out in [78], we have also done some checks to validate the additional infrastructure added for the gravitational recoil calculations in the CLA scheme. First, we have checked that the energy and angular momentum emitted in an equal-mass grazing collision coincide with the ones found by Khanna *et al.* in [47]. Second, we have checked that the recoil velocities that we obtain are consistent with the plots shown by Andrade and Price [44] for the case of head-on collisions from rest of unequal-mass black holes using BL initial data.

We have then performed evolutions for 101 equally spaced values of the symmetric mass ratio η covering the whole range [0, 0.25] for the three values of the physical distance mentioned above, i.e. $D = 3, 3.5, 4M$. The procedure to calculate the bare distance d has been described in the previous subsection. Finally, the linear momentum parameter P is obtained through Eq. (130). For each evolution we have computed the fluxes of energy, angular momentum, and linear momentum carried by the gravitational waves to infinity.

Our initial data only has a few nonzero multipoles contributing to the gravitational radiation emitted. Thus, the expressions for the different fluxes simplify dramati-
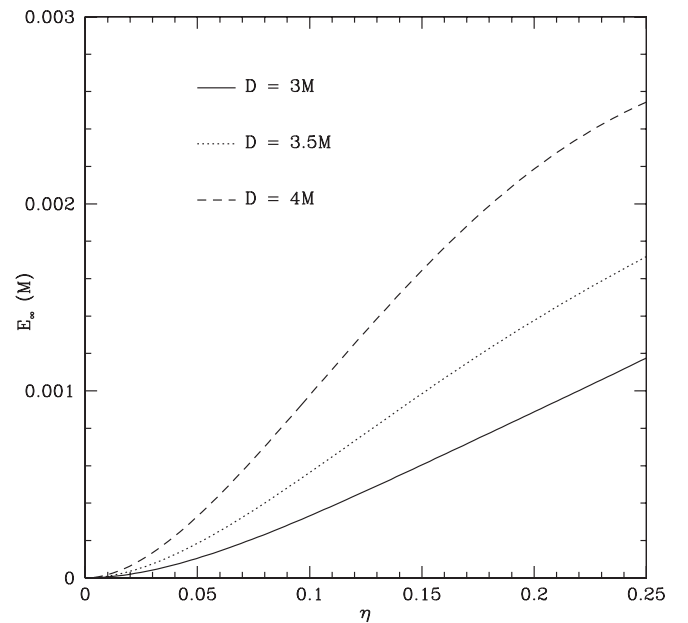

FIG. 4. Energy radiated to infinity in terms of the symmetric mass ratio η for three values of the physical distance: $D = 3, 3.5, 4M$.
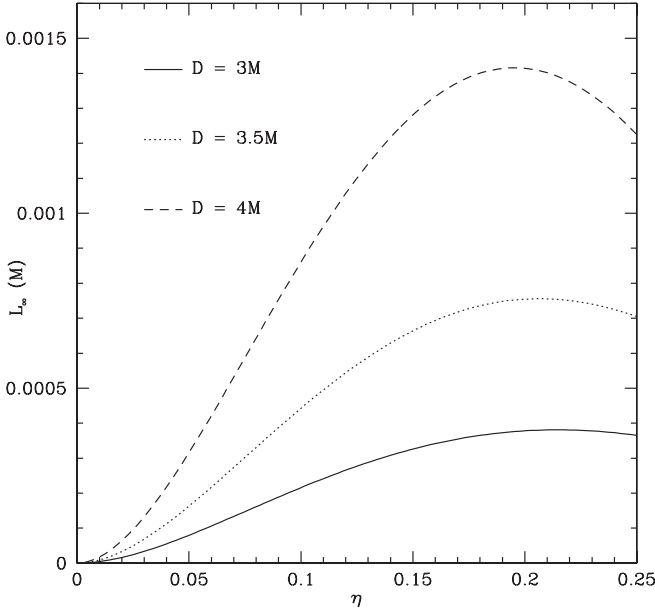
FIG. 5. Angular momentum radiated to infinity in terms of the symmetric mass ratio η for three values of the physical distance: $D = 3, 3.5, 4M$.

cally. The energy flux is given by

$$\dot{E}_{GW} = \frac{3}{8\pi}[(\dot{\Psi}_{ZM}^{2,0})^2 + 2|\dot{\Psi}_{CPM}^{2,1}|^2 + 2|\dot{\Psi}_{ZM}^{2,2}|^2 + 10(|\dot{\Psi}_{ZM}^{3,1}|^2 + |\dot{\Psi}_{ZM}^{3,3}|^2)]. \tag{133}$$

Figure 4 shows the total energy to infinity, given by the integral of Eq. (133) over time, as a function of the symmetric mass ratio. The angular momentum flux also simplifies greatly and becomes

$$\dot{L}_{GW} = \frac{3}{2\pi}\Big\{\Re(\dot{\Psi}_{ZM}^{2,2})\Im(\Psi_{ZM}^{2,2}) - \Im(\dot{\Psi}_{ZM}^{2,2})\Re(\Psi_{ZM}^{2,2})$$
$$+ \frac{5}{2}[\Re(\dot{\Psi}_{ZM}^{3,1})\Im(\Psi_{ZM}^{3,1}) - \Im(\dot{\Psi}_{ZM}^{3,1})\Re(\Psi_{ZM}^{3,1})]$$
$$+ \frac{15}{2}[\Re(\dot{\Psi}_{ZM}^{3,3})\Im(\Psi_{ZM}^{3,3}) - \Im(\dot{\Psi}_{ZM}^{3,3})\Re(\Psi_{ZM}^{3,3})]\Big\}. \tag{134}$$

Note that Eq. (134) does not contain any contributions from the axial modes, since the only nonzero axial mode, $\Psi_{CPM}^{2,1}$, is purely real. Figure 5 shows the total angular momentum radiated to infinity, given by the integral of Eq. (134), as a function of the symmetric mass ratio. Finally, the gravitational waveform also simplifies, and we obtain

$$h_+ = \frac{\sqrt{6}}{r}\{[\Psi_{ZM}^{2,0}{}_{-2}Y^{2,0} + 2\Re(\Psi_{ZM}^{22})\Re(_{-2}Y^{2,2})$$
$$- 2\Im(\Psi_{ZM}^{2,2})\Im(_{-2}Y^{2,2})] + 2\sqrt{5}[\Re(\Psi_{ZM}^{3,1})\Re(_{-2}Y^{3,1})$$
$$- \Im(\Psi_{ZM}^{3,1})\Im(_{-2}Y^{3,1}) + \Re(\Psi_{ZM}^{3,3})\Re(_{-2}Y^{3,3})$$
$$- \Im(\Psi_{ZM}^{3,3})\Im(_{-2}Y^{3,3})]\}, \tag{135}$$

$$h_\times = -\frac{2\sqrt{6}}{r}\Re(\Psi_{CPM}^{2,1})\Re(_{-2}Y^{2,1}), \tag{136}$$

where the definition and some properties of the spin-weighted spherical harmonics $sY^{\ell m}$ are given in Appendix A 3. Note that the ×-polarization consists purely of the axial modes, while the +-polarization contains only polar contributions. Figure 6 shows a typical metric waveform, namely h_+ as a function of time, for an observer located at $\sim 300M$ on the Z-axis (the cross polarization vanishes on this axis).

Let us now concentrate on the main physical quantity of interest, namely, the linear momentum flux, given in Eqs. (57)–(59). These expressions reduce to

$$\dot{P}_{GW}^x = -\frac{1}{2\pi}\sqrt{\frac{5}{14}}\{\sqrt{6}\dot{\Psi}_{ZM}^{2,0}\Re(\dot{\Psi}_{ZM}^{3,1})$$
$$+ \sqrt{15}[\Re(\dot{\Psi}_{ZM}^{2,2})\Re(\dot{\Psi}_{ZM}^{3,3}) + \Im(\dot{\Psi}_{ZM}^{2,2})\Im(\dot{\Psi}_{ZM}^{3,3})]$$
$$- [\Re(\dot{\Psi}_{ZM}^{2,2})\Re(\dot{\Psi}_{ZM}^{3,1}) + \Im(\dot{\Psi}_{ZM}^{2,2})\Im(\dot{\Psi}_{ZM}^{3,1})]\}, \tag{137}$$
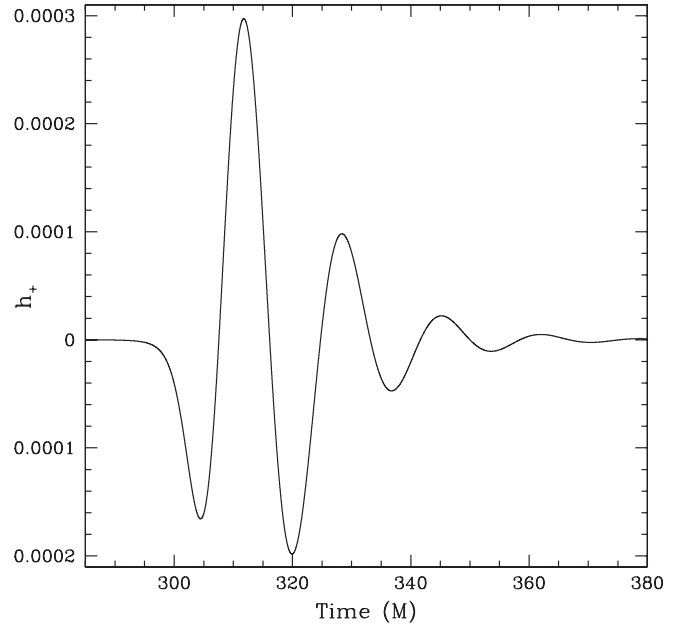

FIG. 6. Metric waveform h_+ for the case $D = 3.5M$ and $\eta = 0.185$ as a function of time. The observer is located at $\sim 300M$ on the Z-axis

$$\dot{P}^y_{GW} = \frac{1}{2\pi}\sqrt{\frac{5}{14}}\{\sqrt{6}\dot{\Psi}^{2,0}_{ZM}\Im(\dot{\Psi}^{3,1}_{ZM})$$
$$+ \sqrt{15}[\Re(\dot{\Psi}^{2,2}_{ZM})\Im(\dot{\Psi}^{3,3}_{ZM}) - \Im(\dot{\Psi}^{2,2}_{ZM})\Re(\dot{\Psi}^{3,3}_{ZM})]$$
$$+ [\Re(\dot{\Psi}^{2,2}_{ZM})\Im(\dot{\Psi}^{3,1}_{ZM}) - \Im(\dot{\Psi}^{2,2}_{ZM})\Re(\dot{\Psi}^{3,1}_{ZM})]\}, \tag{138}$$

$$\dot{P}^z_{GW} = 0. \tag{139}$$

As we can see, there are only contributions from the overlap of polar modes with different ℓ and m. From this flux, the recoil velocity can be obtained by performing the following integration

$$v^i_{recoil} = -\frac{1}{M}\int_{t_i}^{t_f} dt\dot{P}^i, \tag{140}$$

where the integration times, t_i and t_f, are such that the time interval includes essentially all the contribution from the waves to the flux. We can then calculate the magnitude of the recoil velocity simply by

$$v_{recoil} = \sqrt{(v^x)^2 + (v^y)^2 + (v^z)^2}, \tag{141}$$

where $v^z = 0$ in our case, due to the choices made in the initial setup. Figure 7 shows the time derivatives of the master functions that contribute to the recoil velocity for a typical evolution. In this figure, we have separated the real (bottom panel) and the imaginary (top panel) parts of these time derivatives. Observe that the magnitude of the $\ell = 2$

FIG. 8. Linear momentum fluxes, $\dot{P}^x_{GW}$ and $\dot{P}^y_{GW}$, as a function of time, for the case $D = 3.5M$ and $\eta = 0.185$.

modes is much bigger than the one of the $\ell = 3$ modes, as expected. This also gives an indication that the *superposition* of the $\ell = 2$ and $\ell = 3$ is going to be the dominant contribution to the gravitational recoil. The contribution from superpositions involving higher ℓ's is going to be much smaller. Figure 8 shows the linear momentum flux as a function of time. Observe that the magnitude of the
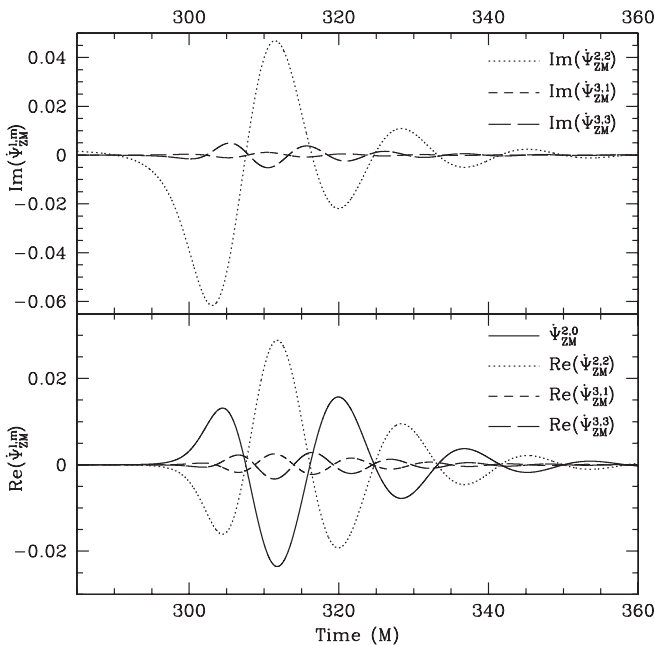

FIG. 7. Time derivate of the Zerilli-Moncrief master function as a function of time, for the case $D = 3.5M$ and $\eta = 0.185$. The plots in the top panel represent the imaginary parts whereas the ones in the bottom panel represent the real parts.
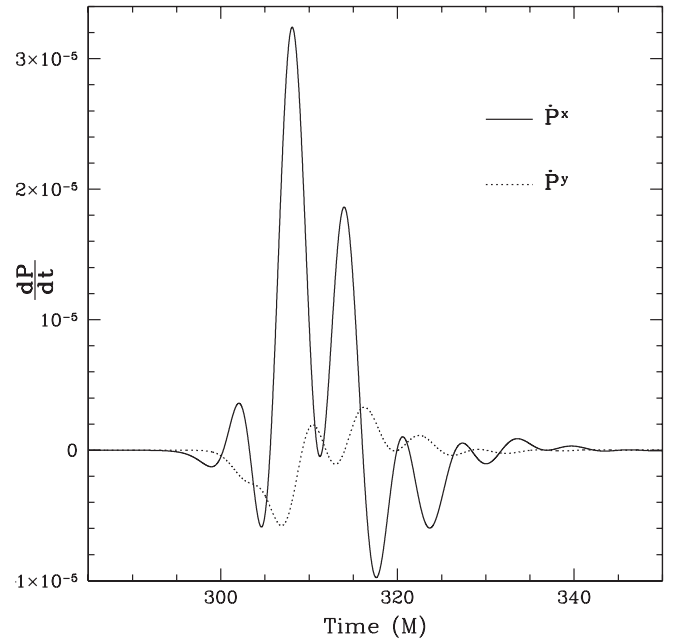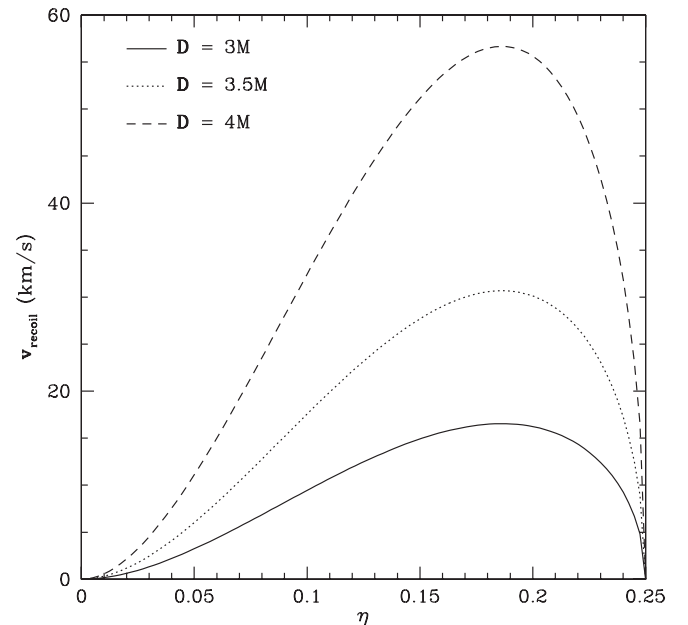

FIG. 9. Magnitude of the recoil velocity in terms of the symmetric mass ratio η for three values of the physical distance: $D = 3, 3.5, 4M$.

x-component is bigger than the *y*-component, which reflects the fact that our configuration corresponds to the transition from merger to plunge. Finally, Fig. 9 presents the magnitude of the recoil velocity as a function of the symmetric mass ratio, for the following initial physical separations: $D = 3, 3.5, 4M$. For all cases studied, the maximum velocity is reached for a symmetric mass ratio of $\eta \sim 0.19$, which agrees with the value reported in Refs. [22,23] up to uncontrolled remainders. Observe that this maximum is not a strong peak, but instead resembles a *plateau*, where this maximum is spread out for a number of *etas*, as also seen in other calculations [22,23].

VI. ESTIMATING THE TOTAL RECOIL

In this section, we discuss the recoil velocities obtained from the evolution of the master functions and produce lower and upper limits for the total recoil velocity. In particular, we will provide analytic approximations to the data and we will also compare these results to other ones already present in the literature.

One of the limitations, and at the same time an advantage, of the CLA scheme is that the initial separation of the black holes must be *sufficiently* small in some well-defined sense. Apart from numerical relativity, this method is the only known one to be capable of producing accurate estimates of physical quantities near plunge. This advantage, however, is a double-edged sword since the method cannot account for the inspiral phase. Actually, the initial separation must even be smaller than that for which the last ISCO exists. Thus, not only is the inspiral phase neglected but also the beginning part of the merger phase.

Because of these limitations, an approximate value for the *total* recoil velocity cannot be provided by the CLA alone, without supplementing it with some other scheme valid when the system is well separated. The PN scheme is well suited for this task and extensive studies have been recently carried out [22,23] to estimate the recoil velocity. The approximate recoil velocity accumulated from infinity up to some final separation in the PN scheme is given by [22]

$$v_{PN} = \frac{464}{105} \eta^2 \frac{\delta m_{\mathrm{PN}}}{m_{\mathrm{PN}}} x_f^4 \left[1 - \left(\frac{452}{87} + \frac{1139}{522} \eta \right) x_f \right.$$
$$+ \frac{309}{58} \pi x_f^{3/2} + \left(\frac{71\,345}{229\,968} + \frac{36\,761}{2088} \eta \right.$$
$$+ \left. \left. \frac{147\,101}{68\,904} \eta^2 \right) x_f^2 \right], \qquad (142)$$

with remainders of $\mathcal{O}(v^5)$. In Eq. (142), $x_f = (m \omega_f)^{2/3}$ is a PN parameter, $m_{\mathrm{PN}} = m_{1,\mathrm{PN}} + m_{2,\mathrm{PN}}$ is the total mass, $m_{1,2,\mathrm{PN}}$ are the masses of the PN point particles, $\eta = m_1 m_2 / m^2$ is the symmetric mass ratio, and $\delta m_{\mathrm{PN}} = m_{1,\mathrm{PN}} - m_{2,\mathrm{PN}}$ is the mass difference. The PN masses $m_{1,2,\mathrm{PN}}$ have been shown to agree, within the PN approximation, with the horizon masses $M_{1,2}$ [72,73] and we make

this identification here. The angular velocity ω is given to $\mathcal{O}(v^4)$ by

$$\omega^2 = \frac{m_{\mathrm{PN}}}{b^3} \left[1 + \frac{m_{\mathrm{PN}}}{b} (\eta - 3) + \frac{m_{\mathrm{PN}}^2}{b^2} \left(6 + \frac{41}{4} \eta + \eta^2 \right) \right], \qquad (143)$$

and ω_f is the angular velocity evaluated at some final coordinate separation b_f. Post-Newtonian theory is usually carried out in harmonic coordinates, which are different from the Schwarzschild coordinate system we use in the CLA scheme. However, sufficiently far from the holes, $D \sim b$, to $\mathcal{O}(v^2)$.

Supplementing the CLA estimate with the PN estimate, we can obtain upper and lower limits on the possible values of the magnitude of the recoil velocity. A lower limit can be obtained via

$$v_{\mathrm{low}} = v_{\mathrm{CLA}}[0, 4M] + v_{\mathrm{PN}}[6M, \infty], \qquad (144)$$

where $v_{\mathrm{PN}}[D_2, \infty]$ is the PN estimate for the recoil velocity of Eq. (142) evaluated at $b_f = D_2$. For this lower limit, we evaluate the PN estimate at the edge of the region of validity of the PN approximation, i.e. $b_f = 6M$, or equivalently $x_f = 6^{-3/2}$, as done in Ref. [22]. This location corresponds to the ISCO of a test particle around a Schwarzschild hole of mass M. One obtains this value of $x_f(b_f = 6M)$ by neglecting terms of $\mathcal{O}(v^2)$ and higher in Eq. (143). If we had included these higher-order terms in ω_f and x_f, the upper bounds would have decreased by approximately 50 km/s. These higher-order terms, however, become large as b becomes smaller, and thus we choose to neglect them to have a conservative upper bound. In Eq. (144), $v_{\mathrm{CLA}}[0, D_1]$ is the estimate of the recoil velocity in the CLA approximation with an initial proper separation of $D = D_1$.

The estimate of v_{low} is a lower limit because it does not take into account the contribution to the gravitational recoil in the region $b \in (4, 6)M$. In this region neither the CLA, nor the PN scheme, is guaranteed to provide an accurate estimate for the recoil. However, it is possible to construct upper limits by modelling either the entire region or part of it with PN and CLA estimates. Such upper limits are given by

$$v_{\mathrm{up,1}} = v_{\mathrm{CLA}}[0, 4M] + v_{\mathrm{PN}}[4M, \infty], \qquad (145)$$

$$v_{\mathrm{up,2}} = v_{\mathrm{CLA}}[0, 5M] + v_{\mathrm{PN}}[5M, \infty]. \qquad (146)$$

These expressions are upper limits because the contribution to the recoil estimated either with PN theory or the CLA approximation in the region $b_f \in (4, 6)M$ is monotonically increasing with b_f.

Equations (144)–(146) require some extra justification and clarification. In general, it is not true that the magnitude of the total recoil can be estimated by adding the magnitude of the integrated momentum flux in the region
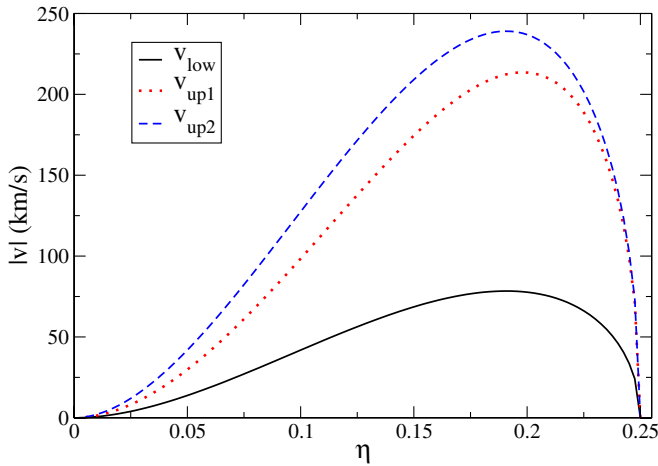
FIG. 10 (color online). Estimated lower (solid curve) and upper limits 1 (dotted line) and 2 (dashed line) for the recoil velocity after a binary black hole merger as a function of the physical symmetric mass ratio. Note that the maximum occurs roughly in the same place, namely $\eta^\star \sim \{0.19, 0.2\}$.

TABLE I. Values of the parameter of the nonlinear fitting for the following models: the CLA with initial separations of $D = \{3, 3.5, 4\}M$; the lower and upper limits of Eqs. (144)–(146); Taylor PN (BQW) and EOB PN (DG) calculations [22,23].

Model	a (km/s)	b	c	Mean square error
$v_{\mathrm{CLA}}[0, 3M]$	1651	-2.94	3.41	0.001
$v_{\mathrm{CLA}}[0, 3.5M]$	3092	-3.02	3.69	0.003
$v_{\mathrm{CLA}}[0, 4M]$	5701	-3.01	3.66	0.008
v_{low}	6907	-2.46	3.03	0.008
$v_{\mathrm{up},1}$	13 927	-1.10	1.55	0.008
$v_{\mathrm{up},2}$	20 897	-2.40	2.83	0.06
v_{BQW}	12 891	0.25	0	10^{-8}
v_{DG}	4483	-0.95	2.68	10^{-10}

$[4M, \infty]$ to that in the region $[0, 4M]$. The important point is that the cut is made at a separation, $D = 4M$, in the regime where the main contribution to the recoil comes from. Then, the main contribution to each recoil velocity vector comes from the region near the cut and hence, the error we made by adding the norms will be relatively small. Independent of this argument we have the inequality $v[0, \infty] \leq v[0, D_{\mathrm{cut}}] + v[D_{\mathrm{cut}}, \infty]$ (with equality when $v[0, D_{\mathrm{cut}}]$ and $v[D_{\mathrm{cut}}, \infty]$ are aligned). In this sense, the proposed upper limit is indeed always an upper limit, irrespective of the orientation of the vectors. As for the lower limit, neglecting the accumulated recoil in the region $[4M, 6M]$ is a very conservative estimate, because there the recoil accumulates greatly. Thus, the issue of the orientation of the vectors will not affect the fact that this is a lower limit, as other recent estimates in the literature confirm.

Figure 10 shows the behavior of these upper limits (dotted and dashed lines, respectively) and the lower limit (solid curve as a function of η). The maximum in these curves occurs roughly at the same symmetric mass ratio, namely $\eta \sim \{0.19, 0.2\}$. The slight disagreement in this maximum is within error bars and rooted in that PN theory predicts it at approximately $\eta \sim 0.2$, while the CLA predicts it at $\eta \sim 0.19$. We should note that the maximum recoil from $v_{\mathrm{CLA}}[0, 4M]$ and $v_{\mathrm{CLA}}[0, 5M]$ is approximately 60 km/s and 190 km/s, while the maximum recoil from $v_{\mathrm{PN}}[4M, \infty]$, $v_{\mathrm{PN}}[5M, \infty]$ and $v_{\mathrm{PN}}[6M, \infty]$ is approximately 160 km/s, 50 km/s, and 20 km/s respectively.

A nonlinear fit can be performed to these curves via Eq. (1)

$$v_{\mathrm{fit}} = a\eta^2\sqrt{1 - 4\eta}(1 + b\eta + c\eta^2),$$

where the fitting parameters a, b, and c are listed in Table I. Observe that the mean square error for all cases is small,

which is an indication that Eq. (1) is a good analytic model for the functional form of the recoil velocity. In this table, we also present the values corresponding to the estimates of Refs. [22] (BQW) and [23] (DG.) Since the predictions of these references are based on analytic formulae, the mean square error can be made arbitrarily small by increasing the number of points in the discretization of the analytic curve.

With the analytic fits to the upper and lower limits, we can construct a curve that is in between these limits with an error given by the distance from the curve to the upper or lower bound. Such a curve is given by Eq. (1) with the following fitting parameters

$$a = \frac{a_{\mathrm{low}} + a_{\mathrm{up}}}{2}, \tag{147}$$

$$b = \frac{a_{\mathrm{low}}b_{\mathrm{low}} + a_{\mathrm{up}}b_{\mathrm{up}}}{a_{\mathrm{low}} + a_{\mathrm{up}}}, \tag{148}$$

$$c = \frac{a_{\mathrm{low}}c_{\mathrm{low}} + a_{\mathrm{up}}c_{\mathrm{up}}}{a_{\mathrm{low}} + a_{\mathrm{up}}}, \tag{149}$$

while the error on this curve is also given by Eq. (1) with the following fitting parameters

$$a = \frac{a_{\mathrm{low}} - a_{\mathrm{up}}}{2}, \tag{150}$$

$$b = \frac{a_{\mathrm{low}}b_{\mathrm{low}} - a_{\mathrm{up}}b_{\mathrm{up}}}{a_{\mathrm{low}} - a_{\mathrm{up}}}, \tag{151}$$

$$c = \frac{a_{\mathrm{low}}c_{\mathrm{low}} - a_{\mathrm{up}}c_{\mathrm{up}}}{a_{\mathrm{low}} - a_{\mathrm{up}}}, \tag{152}$$

where the subscript *low* and *up* stand for the fitting parameters of the lower or upper limit, respectively. This curve is only an alternative way to visualize the upper and lower limits of Fig. 10. The curve is not to be interpreted as the best guess in this work, since in principle, the

recoil velocities present in nature could be closer to either upper or lower limit.

We can now compare these estimates of the recoil velocity with those present in the literature. Figure 11 shows the recoil velocity in units of km/s as a function of the physical symmetric mass ratio as estimated in the literature and by this paper. As is clear from the figure, there are many approaches to calculate this velocity and not all of them agree. The symbols used are the following: squares and triangles stand for the results obtained using black hole perturbation theory in the extreme-mass ratio approximation in Refs. [17,19], respectively; circles stand for the calculations carried out via the Lazarus approach [25]; stars and crosses correspond to the results coming from a full numerical relativistic simulation (PSU stands for Ref. [31] and NASA stands for Ref. [32]); the dotted line and the dashed line correspond to the 2 PN Taylor expansion approach [22] and the 2 PN effective-one-body (EOB) approach [23], respectively. The solid line with error bars is the estimate of Eqs. (149) and (152) that properly condenses the lower and upper limits into one curve. We briefly describe each approach below.

In the PN calculations of Ref. [22], the recoil velocity (dotted line in the figure) and momentum flux are estimated by studying the 2 PN Taylor-expanded radiative moments of a binary system of compact objects, while in Ref. [23] an effective-one-body approach is used (dashed line in the
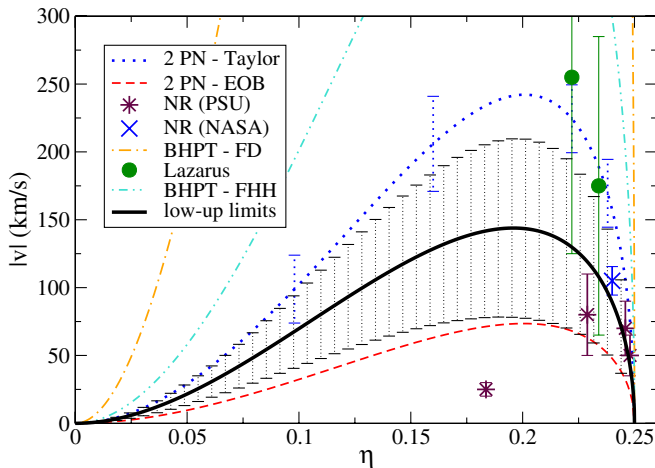

FIG. 11 (color online). Estimates for the recoil velocity (km/s) of the inspiral and merger of a binary system of compact object as a function of the physical symmetric mass ratio parameter. The symbols used are the following: squares and triangles stand for black hole perturbation theory results [17,19]; circles stand for Lazarus results [25]; stars and crosses correspond to full numerical relativistic simulation [31,32]; the dotted line and the dashed line correspond to 2 PN Taylor expansions [22] and 2 PN effective-one-body expansions [23], respectively. The solid black line corresponds to the estimate of this paper, which, together with the error bars, condense both upper and lower limits. Other error bars, when present, correspond to an estimate of some of the error contained in the calculation.

figure.) Post-Newtonian calculations are usually valid only when the binary is weakly gravitating, or equivalently when the orbital separation is greater than the ISCO. In this regime, the recoil velocity (Eq. (142)) has been found to be small for any mass ratio (usually less than 20 km/s), since, as expected, most of the contribution to the recoil comes from the merger part of the inspiral. In Ref. [22] the calculation is extended through the merger by integrating the 2 PN Taylor-expanded momentum flux along a geodesic of the Schwarzschild metric. On the other hand, Ref. [23] uses the effective-one-body Hamiltonian to extend the inspiral through the merger. Both of these approaches have inherent errors that are difficult to estimate without calculating the 3 PN contributions to the recoil velocity.

Black hole perturbation theory has also been used to estimate the recoil velocity in Refs. [17,19]. In these studies, the extreme-mass ratio approximation is adopted (i.e., $Q \ll 1$) and then the system is approximated as a point particle orbiting a black hole. The first study of the recoil velocity using this formalism was performed in Ref. [19] (squares in the figure), but there the gravitational force was treated as Newtonian and only the lowest multipoles were considered. In Ref. [17], these relativistic effects were taken into account, as well as spin, and the velocity estimates were improved (triangles in the figure.) The extreme-mass ratio approximation, however, requires $Q \ll 1$, which allows the exploration of a limited section of the η-space.

A combination of black hole perturbation theory and full numerical relativity (the so-called Lazarus approach) has also been implemented to estimate the recoil velocity [25]. In this case, a full numerical relativistic simulation is carried out until the black holes merge and a single perturbed spinning black hole has formed. Then, this spacetime is used as initial data in a Teukolsky evolution to determine the recoil velocity (circles in the figure.) The error in this calculation is rooted in the interpretation of the initial data as that of a perturbed Kerr spacetime. Finally, there have also been recently full numerical relativistic simulations of binary black hole coalescence [31,32] (shown as stars and crosses, respectively, in the figure.) In this case, the error shown in the figure is assumed to be given only by finite differencing, while the error due to initial data is neglected.

Even though there has been much work in the calculation of the recoil velocity there is still some disagreement. In Fig. 11 we observe that there seem to be three groups of results: one that clusters around the 2 PN Taylor-expanded result; another that is close to the 2 PN effective-one-body result; and a third one that is in between the first two. This disagreement, however, is misleading in several ways. First, some estimates of the recoil velocity quote no error bars, as is the case of the first perturbation theory approach [19] and the 2 PN effective-one-body approach [23].

Second, the error bars that do exist in other calculations are only estimates and could very well have been underestimated. A surprising disagreement is between the PN approaches, since when used to calculate other quantities, such as the angular frequency at the ISCO, they do agree. This disagreement seems to be rooted in the fact that the greatest contribution to the recoil velocity comes from the merger part of the inspiral, where neither extension of the PN approach is guaranteed to be accurate.

Our estimates seem to agree with most results if one accounts for error bars. The results of Refs. [17,19,25] (squares, triangles, and circles in the figure) seem to overestimate the recoil, which is expected in the case of the extreme-mass ratio approximation. The PN results of Refs. [22,23] seem to overestimate and underestimate the recoil, respectively, but they are consistent with our bounds if one takes their error bars (not shown in the figure) into account. The full numerical relativity results seem to overlap with our bounds, although there are only a few of them. We should note that our bound seems to disagree with the full numerical relativistic result for $\eta \sim 0.18$, but that result seems to be an underestimate because of the small initial separation [79].

VII. CONCLUSIONS AND DISCUSSION

We have calculated the recoil velocity after the merger of an unequal-mass binary black hole system using the CLA scheme. This approximation assumes that the black holes are close enough that the system can be approximated by a single perturbed black hole spacetime. In contrast to other approaches, except for full numerical relativity, this approximation allows us to make a valid statement about physical process when the system is close to plunge. Therefore, it is of great interest to use this method for the study of gravitational recoil. However, the CLA has the disadvantage that it cannot be used during the beginning of the merger or the inspiral phases.

Initial data for the CLA can be constructed analytically by mapping data suitable for a binary black hole inspiral to that of a single perturbed hole. With such initial data, the Cunningham-Price-Moncrief and the Zerilli-Moncrief master functions can be numerically evolved from some initial proper separation through ringdown. These gauge-invariant master functions contain all the information necessary to evaluate the gravitational metric waveforms and, thus, the energy, angular momentum, and linear momentum fluxes carried away from the system.

The results obtained can be summarized as follows. First, the maximum recoil velocity obtained in the CLA scheme is of $v \sim 57$ km/s for the maximum initial separation allowed by this method ($D = 4M$). This maximum occurs at a symmetric mass ratio of $\eta \sim 0.19$. By supplementing this estimate with PN ones valid in the inspiral regime, we obtain lower and upper bounds with maxima of $v \sim 80$ km/s and $v \sim 215$ km/s, respectively. We have

further provided nonlinear analytic fit functions that conveniently parametrize these bounds, together with the results from the CLA, and other results in the literature. These results also suggest that there is a region around $D \sim \{4, 6\}M$ that greatly contributes to the recoil, but can only be poorly modeled by current approximation schemes.

Ultimately, the estimates presented here suffer from the same predicaments as other calculations. Because of its analytical nature, the CLA relies on certain assumptions that do not hold over the entire history of the binary. Such assumptions introduce an error in the estimated recoil that is difficult to quantify. In particular, the assumptions made here are the following: close separations; slow motion; simple initial data. The close-limit assumption is essential to allow a mapping of a binary inspiral to a single perturbed spacetime. The slow-motion approximation supplements the close-limit assumption and can, in principle, be improved on in future extensions of this work. The choice of initial data is assumed to represent the gravitational content of some initial slice, although we know that this fails even at large separation because it does not agree with the deviations from conformal flatness predicted by PN theory. Moreover, it does not contain any radiation, which is not what it should be expected for initial data corresponding to a snapshot of the orbital evolution. Because of these assumptions, the estimate of the recoil velocity will be contaminated by some error. However, experience in CLA calculations indicates that the error made only overestimates the physical quantities calculated, relative to full numerical simulations [39,47,80].

Future work will concentrate on extending this approach to second order in P and to other, more realistic, initial data sets [81,82]. Ultimately, it would be interesting to compare the CLA approach directly to full numerical relativistic simulations in an attempt to determine the region of validity of the CLA more accurately. Another possibility is to use a multiparameter perturbation scheme (see [83–86]) where perturbations in the linear momentum and separation parameters can be cleanly separated at the different perturbative orders.

Carlos Lousto, Ben Owen, and Ulrich Sperhake for enlightening discussions and comments. No. PHY-05-55628.

Note added.—After this paper was submitted, full numerical relativity estimates have appeared [95], and a best-bet estimate based on our scheme, which includes some refinements in the PN part with respect to the present paper, has been compared to them in [96]. The agreement between them is remarkable and supports the approach presented in this paper.

APPENDIX A: CONVENTIONS FOR SPECIAL FUNCTIONS

In this appendix, we describe the conventions we use for the special functions presented in this paper, and we also present some important properties of such functions.

1. Special polynomials

The expression for the associated Legendre polynomials that we are using in this paper is the following

$$P_\ell^m(x) = \frac{(-1)^{\ell+m}}{2^\ell \ell!}(1 - x^2)^{m/2}\frac{d^{\ell+m}}{dx^{\ell+m}}(1 - x^2)^\ell, \quad \text{(A1)}$$

where ℓ is a non-negative integer and m is an integer restricted to the following range: $m \in (-\ell, -(\ell - 1), \ldots, \ell - 1, \ell)$.

Gegenbauer polynomials, also known as ultraspherical harmonics [57], are generalization of the Legendre polynomial for higher dimensional spaces. They can be written in terms of other special functions, as in

$$C_n^{(\lambda)} = \frac{\Gamma(\lambda + 1/2)}{\Gamma(2\lambda)}\frac{\Gamma(n + 2\lambda)}{\Gamma(n + \lambda + 1/2)}P_n^{(\lambda-1/2,\lambda-1/2)}, \quad \text{(A2)}$$

where λ is a real number, n is a positive integer, Γ is the Gamma function, and $P_n^{(\lambda_1,\lambda_2)}$ are the Jacobi polynomials [57]. There are also recursion relations for these polynomials, but we will not present them here. Instead, we will provide the first few Gegenbauer polynomials

$$C_0^{(\lambda)}(x) = 1, \quad \text{(A3)}$$

$$C_1^{(\lambda)}(x) = 2\lambda x, \quad \text{(A4)}$$

$$C_2^{(\lambda)}(x) = -\lambda[1 - 2(1 + \lambda)x^2], \quad \text{(A5)}$$

$$C_3^{(\lambda)}(x) = -2\lambda(1 + \lambda)x\left[1 - \frac{2}{3}(2 + \lambda)x^2\right]. \quad \text{(A6)}$$

These polynomials allow for the far field expansion of potentials that scale as $|\vec{x} - \vec{x}_0|^{-\alpha}$ to arbitrary order.

2. Spherical harmonics

The scalar spherical harmonics are solutions of the eigenvalue problem described by the following equation

$$\Omega^{ab}Y_{:ab}^{\ell m} + \ell(\ell + 1)Y^{\ell m} = 0, \quad \text{(A7)}$$

where (ℓ, m) have the same range of values as in the associated Legendre polynomials above. In this paper we use the conventions of [77,87] to define specifically the solutions of Eq. (A7). The precise expression is given by

$$Y^{\ell m}(\theta, \varphi) = \sqrt{\frac{2\ell + 1}{4\pi}\frac{(\ell - m)!}{(\ell + m)!}}P_\ell^m(\cos\theta)e^{im\varphi}. \quad \text{(A8)}$$

The scalar spherical harmonics form an orthonormal basis on the two-sphere, that is

$$\int_{S^2} d\Omega Y^{\ell m}\bar{Y}^{\ell'm'} = \delta^{\ell\ell'}\delta^{mm'}, \quad \text{(A9)}$$

where δ^{ab} denotes the Kronecker delta. The vector spherical harmonics are defined in terms of the scalar ones as in Eq. (37), and from this definition we can derive the following orthogonality relations:

$$\int_{S^2} d\Omega\, \Omega^{ab}Y_a^{\ell m}\bar{Y}_b^{\ell'm'} = \ell(\ell + 1)\delta^{\ell\ell'}\delta^{mm'}, \quad \text{(A10)}$$

$$\int_{S^2} d\Omega\, \Omega^{ab}S_a^{\ell m}\bar{S}_b^{\ell'm'} = \ell(\ell + 1)\delta^{\ell\ell'}\delta^{mm'}, \quad \text{(A11)}$$

$$\int_{S^2} d\Omega\, \Omega^{ab}Y_a^{\ell m}\bar{S}_b^{\ell'm'} = 0. \quad \text{(A12)}$$

The (symmetric) tensor spherical harmonics used in this paper are also constructed from the scalar ones by means of Eqs. (38) and (39), from where the following orthogonality relations can be deduced:

$$\int_{S^2} d\Omega\, \Omega^{ac}\Omega^{bd}Y_{ab}^{\ell m}\bar{Y}_{cd}^{\ell'm'} = 2\delta^{\ell\ell'}\delta^{mm'}, \quad \text{(A13)}$$

$$\int_{S^2} d\Omega\, \Omega^{ac}\Omega^{bd}Z_{ab}^{\ell m}\bar{Z}_{cd}^{\ell'm'} = \frac{(\ell + 2)!}{2(\ell - 2)!}\delta^{\ell\ell'}\delta^{mm'}, \quad \text{(A14)}$$

$$\int_{S^2} d\Omega\, \Omega^{ac}\Omega^{bd}S_{ab}^{\ell m}\bar{S}_{cd}^{\ell'm'} = \frac{(\ell + 2)!}{2(\ell - 2)!}\delta^{\ell\ell'}\delta^{mm'}, \quad \text{(A15)}$$

$$\int_{S^2} d\Omega\, \Omega^{ac}\Omega^{bd}Z_{ab}^{\ell m}\bar{S}_{cd}^{\ell'm'} = 0, \quad \text{(A16)}$$

and

$$\Omega^{ac}\Omega^{bd}Z_{ab}^{\ell m}Y_{cd}^{\ell'm'} = \Omega^{ac}\Omega^{bd}S_{ab}^{\ell m}Y_{cd}^{\ell'm'} = 0. \quad \text{(A17)}$$

3. Spin-weighted scalar spherical harmonics

Spin-weighted scalar spherical harmonics are another basis to expand functions on the 2-sphere. They can be defined by the following general formula [88]

$$
{}_sY^{lm}(\theta, \varphi) = \begin{cases} \left[\frac{(l-s)!}{(l+s)!}\right]^{1/2}\hat{\eth}^s Y^{lm}, & 0 < s < l, \\ (-1)^s\left[\frac{(l+s)!}{(l-s)!}\right]^{1/2}\check{\eth}^{-s}Y^{lm}, & -l < s < 0, \\ 0, & l < |s|, \end{cases}
$$
(A18)

where $\hat{\eth}$ ($\check{\eth}$) is a ladder operator, usually called the edth operator, that raises (lowers) in a unity the spin weight of any quantity. Its action on a scalar Q can be expressed in the following way [88,89]

$$
\hat{\eth}Q = m^a\partial_a Q - \frac{s}{2}(\bar{m}^a m^b \nabla_b m_a)Q,
$$
(A19)

$$
\check{\eth}Q = \bar{m}^a\partial_a Q + \frac{s}{2}(m^a \bar{m}^b \nabla_b \bar{m}_a)Q,
$$
(A20)

where s is the spin weight of Q and $(m^a, \bar{m}^a)$ is a null complex basis on the 2-sphere $(\Omega_{ab}m^a m^b = 0, \Omega_{ab}m^a \bar{m}^b = 1)$. It is worth noting that the action of the edth depends explicitly on the spin weight of the quantity on which it acts. Taking $m^a = \frac{1}{\sqrt{2}}[1, \frac{i}{\sin\theta}]$, we can write the edth operator as [89]

$$
\hat{\eth} = \frac{1}{\sqrt{2}}\left[\partial_\theta + \frac{i}{\sin\theta}\partial_\varphi - \frac{s}{2}\frac{\cos\theta}{\sin\theta}\right],
$$
(A21)

$$
\check{\eth} = \frac{1}{\sqrt{2}}\left[\partial_\theta - \frac{i}{\sin\theta}\partial_\varphi + \frac{s}{2}\frac{\cos\theta}{\sin\theta}\right].
$$
(A22)

It is important to mention that these definitions are applicable only to integer powers of the spin weight. A generalized definition for half-integer powers of s exists but will not be discussed here (see [88]).

In this paper we are interested in the $s = -2$ case, for which the definition of the spin-weighted spherical harmonics reduces to [90]

$$
{}_{-2}Y^{\ell m} = 2\sqrt{\frac{(\ell-2)!}{(\ell+2)!}}Z^{\ell m}_{ab}\bar{m}^a\bar{m}^b.
$$
(A23)

APPENDIX B: RELATIONS WITH THE REGGE-WHEELER PARAMETRIZATION OF THE PERTURBATIONS

For the sake of completeness, we give here the relations between our parametrization of the metric perturbations and the one used by Regge and Wheeler [58]. For polar modes (our notation is on the left column and the one of Regge and Wheeler is on the right one) we have

$$
(h^{\ell m}_{AB}) \leftrightarrow \begin{pmatrix} fH^{\ell m}_0 & H^{\ell m}_1 \\ * & f^{-1}H^{\ell m}_2 \end{pmatrix},
$$
(B1)

$$
p^{\ell m}_A \leftrightarrow (h^{\ell m}_t, h^{\ell m}_r),
$$
(B2)

$$
K^{\ell m} \leftrightarrow K^{\ell m} - \frac{\ell(\ell+1)}{2}G^{\ell m},
$$
(B3)

$$
G^{\ell m} \leftrightarrow G^{\ell m},
$$
(B4)

and for axial modes

$$
(h^{\ell m}_A) \leftrightarrow -(h^{\ell m}_0, h^{\ell m}_1),
$$
(B5)

$$
H^{\ell m} \leftrightarrow -h^{\ell m}_2.
$$
(B6)

The expressions for the master functions, in Schwarzschild coordinates, in terms of the parametrization of Regge and Wheeler are:

$$
\Psi^{\ell m}_{\text{ZM}} = \frac{r}{1+\lambda_\ell}\left[K^{\ell m} + \frac{f}{\Lambda_\ell}(H^{\ell m}_2 - r\partial_r K^{\ell m})\right] \\ - \frac{2f}{\Lambda_\ell}\left(h^{\ell m}_1 - \frac{r^2}{2}\partial_r G^{\ell m}\right),
$$
(B7)

$$
\Psi^{\ell m}_{\text{RW}} = \frac{f}{r}\left(h^{\ell m}_1 - \frac{1}{2}\partial_r h^{\ell m}_2 + \frac{1}{r}h^{\ell m}_2\right),
$$
(B8)

$$
\Psi^{\ell m}_{\text{CPM}} = \frac{r}{\lambda_\ell}\left(\dot{h}^{\ell m}_1 - \partial_r h^{\ell m}_0 + \frac{2}{r}h^{\ell m}_0\right).
$$
(B9)

APPENDIX C: ON THE DERIVATION OF THE LINEAR MOMENTUM FLUX FORMULA

In order to obtain Eqs. (57)–(59) from Eq. (55) we need to use the decompositions of products of spherical harmonics in single harmonics typical of problems that deal with angular momentum coupling (for accounts dealing with this problem see [67], where multipole expansions of gravitational radiation in different sets of harmonics are described; see [91] for a recent systematic treatment of higher-order perturbation theory where these issues are also treated).

Introducing Eq. (54) into Eq. (55), using that any spherical harmonic $\mathcal{S}^{\ell m}$ has the property $\mathcal{S}^{\ell, -m} = (-1)^m\bar{\mathcal{S}}^{\ell m}$, and the fact that $Z^{\ell m}_{ab}$ is symmetric and traceless we get

$$
\dot{P}^{\,k}_{GW} = \frac{1}{32\pi}\sum_{\substack{\ell\geq 2, m, \\ \ell'\geq 2, m'}}(\dot{\Psi}^{\ell m}_{\text{ZM}}\dot{\bar{\Psi}}^{\ell'm'}_{\text{ZM}} + \dot{\Psi}^{\ell m}_{\text{CPM}}\dot{\bar{\Psi}}^{\ell'm'}_{\text{CPM}}) \\ \times \int_{S^2}d\Omega\,\hat{r}^k_{obs}Z^{\ell m}_{ab}\bar{Z}^{\ell'm'}_{cd}\Omega^{ac}\Omega^{bd}.
$$
(C1)

At this point everything reduces to evaluate the integral on the 2-sphere. To that end, the starting point is the well-known formula [92]

$$
Y^{\ell m}Y^{\ell'm'} = \sum_{L,M}\sqrt{\frac{(2\ell+1)(2\ell'+1)(2L+1)}{4\pi}} \\ \times \begin{pmatrix} \ell & \ell' & L \\ m & m' & M \end{pmatrix}\begin{pmatrix} \ell & \ell' & L \\ 0 & 0 & 0 \end{pmatrix}\bar{Y}^{LM},
$$
(C2)

where the objects with the round brackets are the $3j$-Wigner symbols, which are related to the Clebsch-Gordon coefficients. They are subject to certain *selection* rules, namely, (ℓ, m), (ℓ', m'), and (L, M) are integers with the usual ranges of values; $m + m' + M = 0$; and the

triangular inequality $|\ell - \ell'| \leq L \leq \ell + \ell'$. By using (C2) and the definition of $Z_{ab}^{\ell m}$ [Eq. (38)] we find the following relationship

$$Z_{ab}^{\ell m}\bar{Z}_{cd}^{\ell'm'}\Omega^{ac}\Omega^{bd} = \sum_{L,M} C(\ell, \ell', L)\sqrt{\frac{(2\ell + 1)(2\ell' + 1)(2L + 1)}{4\pi}}\begin{pmatrix} \ell & \ell' & L \\ m & m' & M \end{pmatrix}\begin{pmatrix} \ell & \ell' & L \\ 0 & 0 & 0 \end{pmatrix}\bar{Y}^{LM}, \tag{C3}$$

where $C(\ell, \ell', L)$ is a constant given by

$$C(\ell, \ell', L) = \frac{1}{4}\{L^2(L + 1)^2 + \ell^2(\ell + 1)^2 + \ell'^2(\ell' + 1)^2 + 2L(L + 1) - 2[\ell(\ell + 1) + \ell'(\ell' + 1)][L(L + 1) + 1]\}. \tag{C4}$$

Then, since the components of $\hat{r}_{\text{obs}}^k$ are linear in $Y^{1,m}$, the integral that appears in Eq. (C1) is now straightforward. In order to get Eqs. (57)–(59) we just need to use the selection rules of the $3 - j$ Wigner symbols and the following additional properties:

$$\begin{pmatrix} j_1 & j_2 & j_1 + j_2 \\ m_1 & m_2 & -M \end{pmatrix} = (-1)^{j_1 - j_2 + M}\left[\frac{(2j_1)!(2j_2)!}{(2j_1 + 2j_2 + 1)!}\frac{(j_1 + j_2 + M)!(j_1 + j_2 - M)!}{(j_1 + m_1)!(j_1 - m_1)!(j_2 + m_2)!(j_2 - m_2)!}\right]^{1/2}, \tag{C5}$$

$$\begin{pmatrix} j_1 & j_2 & j \\ 0 & 0 & 0 \end{pmatrix} = \begin{cases} (-1)^g\left[\frac{(2g-2j_1)!(2g-2j_2)!(2g-2j)!}{(2g+1)!}\right]^{1/2}\frac{g!}{(g-j_1)!(g-j_2)!(g-j)!}, & \text{if } J = 2g, \\ 0, & \text{if } J = 2g + 1, \end{cases} \tag{C6}$$

where $J = j_1 + j_2 + j$.

APPENDIX D: DETERMINING EXTREMAL SURFACES IN THE BRILL-LINDQUIST BINARY BLACK HOLE DATA

We are interested in finding the location of the extremal surfaces that surround the individual holes in the BL binary black hole initial data that we are using in this paper. When the holes are separated enough these surfaces form the apparent horizon of the initial data (since we are neglecting the extrinsic curvature the data is time symmetric). If we put the two holes close enough, another maximal surface enclosing the two holes appears and becomes the apparent horizon, and then, the two individual maximal surfaces are called marginally trapped surfaces.

Following Bishop [93,94], in order to look for maximal surfaces in the BL data it is very convenient to exploit the cylindrical symmetry of the configuration by expressing the metric in cylindrical coordinates (for coherence with the conventions of the paper we choose the axis of symmetry to be the X-axis): $x = x$, $y = \rho\cos\vartheta$, $z = \rho\sin\vartheta$. Then, the line element of Eq. (2) becomes:

$$ds^2 = \Phi^4(\rho, x)(d\rho^2 + \rho^2 d\vartheta^2 + dx^2), \tag{D1}$$

where now

$$\Phi = 1 + \frac{m_1}{2\sqrt{\rho^2 + (x - X_1)^2}} + \frac{m_2}{2\sqrt{\rho^2 + (x - X_2)^2}}. \tag{D2}$$

Moreover, the problem of finding the extremal surfaces

reduces to that of finding a path $(\rho(\lambda), x(\lambda))$ in the subspace (ρ, x). The area of a surface with cylindrical symmetry can be written as

$$\mathcal{A} = 2\pi\int_{\lambda_1}^{\lambda_2}\rho\Phi^4\sqrt{\dot{\rho}^2 + \dot{x}^2}d\lambda, \tag{D3}$$

where the dots denote differentiation along the path, that is, $d/d\lambda$, and (λ_1, λ_2) are the intersections of the surface with the symmetry axis X. The equations for the path $(\rho(\lambda), x(\lambda))$ are found by extremizing the area, $\delta\mathcal{A} = 0$, Bishop [93,94] took λ to be an affine parameter, that is, such that $\mathcal{A} = 2\pi(\lambda_2 - \lambda_1)$. We have fixed λ in such a way the ordinary differential equations for $(\rho(\lambda), x(\lambda))$ are simple and amenable for numerical computations. In particular, we have chosen λ so that

$$\sqrt{\dot{\rho}^2 + \dot{x}^2} = \rho\Phi^4, \tag{D4}$$

which is a constraint preserved by the Euler-Lagrange equations that we obtain from $\delta\mathcal{A} = 0$:

$$\ddot{\rho} = -\partial_\rho\mathcal{V}, \tag{D5}$$

$$\ddot{x} = -\partial_x\mathcal{V}, \tag{D6}$$

where the *potential* $\mathcal{V}$ is given by

$$\mathcal{V}(\rho, x) = \frac{1}{2}\rho^2\Phi^8. \tag{D7}$$

[1] LIGO, www.ligo.caltech.edu.
[2] VIRGO, www.virgo.infn.it.
[3] GEO600, www.geo600.uni-hannover.de.
[4] TAMA, tamago.mtk.nao.ac.jp.
[5] LISA, http://lisa.jpl.nasa.gov.
[6] B. Binggeli and H. Jerjen, Astron. Astrophys. **333**, 17 (1998).
[7] B. Binggeli, F. Barazza, and H. Jerjen, Astron. Astrophys. **359**, 447 (2000).
[8] D. Merritt, M. Milosavljevic, M. Favata, S. A. Hughes, and D. E. Holz, Astrophys. J. **607**, L9 (2004).
[9] M. G. Haehnelt, M. B. Davies, and M. J. Rees, Mon. Not. R. Astron. Soc. **366**, L22 (2006).
[10] Z. Haiman, Astrophys. J. **613**, 36 (2004).
[11] W. Bonnor and M. Rotenberg, Proc. R. Soc. A **265**, 109 (1961).
[12] A. Papapetrou, Ann. Inst. Henri Poincare **14**, 79 (1962).
[13] A. Peres, Phys. Rev. **128**, 2471 (1962).
[14] J. D. Bekenstein, Astrophys. J. **183**, 657 (1973).
[15] I. H. Redmount and M. J. Rees, Comments Astrophys. **14**, 165 (1989).
[16] A. G. Wiseman, Phys. Rev. D **46**, 1517 (1992).
[17] M. Favata, S. A. Hughes, and D. E. Holz, Astrophys. J. **607**, L5 (2004).
[18] M. J. Fitchett, Mon. Not. R. Astron. Soc. **203**, 1049 (1983).
[19] M. J. Fitchett and S. Detweiler, Mon. Not. R. Astron. Soc. **211**, 933 (1984).
[20] K.-I. Oohara and T. Nakamura, Phys. Lett. A **94**, 349 (1983).
[21] T. Nakamura and M. P. Haugan, Astrophys. J. **269**, 292 (1983).
[22] L. Blanchet, M. S. S. Qusailah, and C. M. Will, Astrophys. J. **635**, 508 (2005).
[23] T. Damour and A. Gopakumar, Phys. Rev. D **73**, 124006 (2006).
[24] S. A. Hughes, M. Favata, and D. E. Holz, in *Proceedings of the MPA/MPE/ESO/USM Conference: Growing Black Holes: Accretion in a Cosmological Context, Garching, Germany, 2004*, edited by A. Merloni, S. Nayakshin, and R. A. Sunyaev (Springer-Verlag, Berlin, 2005), p. 333.
[25] M. Campanelli, Classical Quantum Gravity **22**, S387 (2005).
[26] P. Anninos and S. Brandt, Phys. Rev. Lett. **81**, 508 (1998).
[27] S. Brandt and P. Anninos, Phys. Rev. D **60**, 084005 (1999).
[28] F. Pretorius, Phys. Rev. Lett. **95**, 121101 (2005).
[29] M. Campanelli, C. O. Lousto, P. Marronetti, and Y. Zlochower, Phys. Rev. Lett. **96**, 111101 (2006).
[30] J. G. Baker, J. Centrella, D.-I. Choi, M. Koppitz, and J. van Meter, Phys. Rev. Lett. **96**, 111102 (2006).
[31] F. Herrmann, D. Shoemaker, and P. Laguna, gr-qc/0601026.
[32] J. G. Baker *et al.*, astro-ph/0603204.
[33] R. H. Price and J. Pullin, Phys. Rev. Lett. **72**, 3297 (1994).
[34] P. Anninos, D. Hobill, E. Seidel, L. Smarr, and W.-M. Suen, Phys. Rev. Lett. **71**, 2851 (1993).
[35] P. Anninos, R. H. Price, J. Pullin, E. Seidel, and W.-M. Suen, Phys. Rev. D **52**, 4462 (1995).
[36] R. J. Gleiser, C. O. Nicasio, R. H. Price, and J. Pullin, Phys. Rev. Lett. **77**, 4483 (1996).

[37] R. J. Gleiser, C. O. Nicasio, R. H. Price, and J. Pullin, Phys. Rep. **325**, 41 (2000).
[38] W. Krivan and R. H. Price, Phys. Rev. Lett. **82**, 1358 (1999).
[39] C. O. Nicasio, R. J. Gleiser, R. H. Price, and J. Pullin, Phys. Rev. D **59**, 044024 (1999).
[40] R. J. Gleiser and A. E. Dominguez, Phys. Rev. D **65**, 064018 (2002).
[41] G. Khanna, Phys. Rev. D **63**, 124007 (2001).
[42] O. Sarbach, M. Tiglio, and J. Pullin, Phys. Rev. D **65**, 064026 (2002).
[43] G. Khanna, Phys. Rev. D **66**, 064004 (2002).
[44] Z. Andrade and R. H. Price, Phys. Rev. D **56**, 6336 (1997).
[45] U. H. Gerlach and U. K. Sengupta, Phys. Rev. D **19**, 2268 (1979).
[46] U. H. Gerlach and U. K. Sengupta, Phys. Rev. D **22**, 1300 (1980).
[47] G. Khanna, R. Gleiser, R. Price, and J. Pullin, New J. Phys. **2**, 3 (2000).
[48] A. Lichnerowicz, J. Math. Pures Appl. **23**, 37 (1944).
[49] J. York, Jr., Phys. Rev. Lett. **26**, 1656 (1971).
[50] J. York, Jr., Phys. Rev. Lett. **28**, 1082 (1972).
[51] J. York, Jr., J. Math. Phys. (N.Y.) **14**, 456 (1973).
[52] G. B. Cook, Living Rev. Relativity **3**, 5 (2000).
[53] J. M. Bowen and J. W. York, Phys. Rev. D **21**, 2047 (1980).
[54] C. W. Misner, Phys. Rev. **118**, 1110 (1960).
[55] D. R. Brill and R. W. Lindquist, Phys. Rev. **131**, 471 (1963).
[56] E. U. Condon and G. H. Shortley, *The Theory of Atomic Spectra* (Cambridge University Press, Cambridge, England, 1970).
[57] Arfken and Weber, *Mathematical Methods for Physicists* (Academic, New York, 2001).
[58] T. Regge and J. A. Wheeler, Phys. Rev. **108**, 1063 (1957).
[59] F. J. Zerilli, Phys. Rev. Lett. **24**, 737 (1970).
[60] V. Moncrief, Ann. Phys. (N.Y.) **88**, 323 (1974).
[61] K. Martel and E. Poisson, Phys. Rev. D **71**, 104003 (2005).
[62] C. T. Cunningham, R. H. Price, and V. Moncrief, Astrophys. J. **224**, 643 (1978).
[63] S. Jhingan and T. Tanaka, Phys. Rev. D **67**, 104018 (2003).
[64] R. A. Isaacson, Phys. Rev. **166**, 1263 (1968).
[65] R. A. Isaacson, Phys. Rev. **166**, 1272 (1968).
[66] C. W. Misner, K. Thorne, and J. A. Wheeler, *Gravitation* (Freeman, San Francisco, 1973).
[67] K. S. Thorne, Rev. Mod. Phys. **52**, 299 (1980).
[68] J. N. Goldberg, A. J. Macfarlane, E. T. Newman, F. Rohrlich, and E. C. G. Sudarshan, J. Math. Phys. (N.Y.) **8**, 2155 (1967).
[69] R. Arnowitt, S. Deser, and C. W. Misner, in *Gravitation: An Introduction to Current Research*, edited by L. Witten (Wiley, New York, 1962), p. 227.
[70] A. M. Abrahams and R. H. Price, Phys. Rev. D **53**, 1963 (1996).
[71] R. Beig, *Mathematical and Quantum Aspects of Relativity and Cosmology*, Lecture Notes in Physics Vol. 537 (Springer-Verlag, Berlin, 2000), p. 55.
[72] L. Blanchet, G. Faye, and B. Ponsot, Phys. Rev. D **58**, 124002 (1998).
[73] L. Blanchet, Phys. Rev. D **68**, 084002 (2003).

[74] C. O. Lousto and R. H. Price, Phys. Rev. D **55**, 2124 (1997).

[75] R. Bulirsch and J. Stoer, Numer. Math. **8**, 1 (1966).

[76] J. Stoer and R. Bulirsch, *Introduction to Numerical Analysis* (Springer-Verlag, Berlin, 1993).

[77] W. H. Press, B. P. Flannery, S. A. Teukolsky, and W. T. Vetterling, *Numerical Recipes: The Art of Scientific Computing* (Cambridge University Press, Cambridge, England, 1992).

[78] C. F. Sopuerta and P. Laguna, Phys. Rev. D **73**, 044028 (2006).

[79] F. Herrmann (private communication).

[80] G. Khanna *et al.*, Phys. Rev. Lett. **83**, 3581 (1999).

[81] N. Yunes, W. Tichy, B. J. Owen, and B. Bruegmann, Phys. Rev. D **74**, 104011 (2006).

[82] N. Yunes and W. Tichy, Phys. Rev. D **74**, 064013 (2006.

[83] M. Bruni, L. Gualtieri, and C. F. Sopuerta, Classical Quantum Gravity **20**, 535 (2003).

[84] C. F. Sopuerta, M. Bruni, and L. Gualtieri, Phys. Rev. D **70**, 064002 (2004).

[85] A. Passamonti, M. Bruni, L. Gualtieri, and C. F. Sopuerta, Phys. Rev. D **71**, 024022 (2005).

[86] A. Passamonti, M. Bruni, L. Gualtieri, A. Nagar, and C. F. Sopuerta, Phys. Rev. D **73**, 084010 (2006).

[87] M. Abramowitz and I. A. Stegun, *Handbook of Mathematical Functions with Formulas, Graphs, and Mathematical Tables* (Dover, New York, 1972).

[88] J. Stewart, *Advanced General Relativity* (Cambridge University Press, Cambridge, England, 1990).

[89] T. Dray, J. Math. Phys. (N.Y.) **26**, 1030 (1985).

[90] K. Martel, Ph.D. thesis, The University of Guelph, 2003.

[91] D. Brizuela, J. M. Martin-Garcia, and G. A. M. Marugan, Phys. Rev. D **74**, 044039 (2006).

[92] A. Messiah, *Quantum Mechanics* (North-Holland, Amsterdam, 1962), Vol. 2.

[93] N. T. Bishop, Gen. Relativ. Gravit. **14**, 717 (1982).

[94] N. T. Bishop, Gen. Relativ. Gravit. **16**, 589 (1984).

[95] J. A. Gonzalez, U. Sperhake, B. Bruegmann, M. Hannam, and S. Husa, gr-qc/0610154.

[96] C. F. Sopuerta, N. Yunes, and P. Laguna, astro-ph/0611110.

[97] GRTensorII, this is a package which runs within Maple but distinct from packages distributed with Maple. It is distributed freely on the World-Wide-Web from the address: http://grtensor.org.